



**HAL**  
open science

# Impact of Adsorption Kinetics on Pollutant Dispersion in Water Flowing in Nanopores: A Lattice Boltzmann Approach to Stationary and Transient Conditions

Zaineb Zaafouri, Guillaume Batôt, Carlos Nieto-Draghi, Benoit Coasne,  
Daniela Bauer

► **To cite this version:**

Zaineb Zaafouri, Guillaume Batôt, Carlos Nieto-Draghi, Benoit Coasne, Daniela Bauer. Impact of Adsorption Kinetics on Pollutant Dispersion in Water Flowing in Nanopores: A Lattice Boltzmann Approach to Stationary and Transient Conditions. *Advances in Water Resources*, 2022, 162, pp.104143. 10.1016/j.advwatres.2022.104143 . hal-03619397

**HAL Id: hal-03619397**

**<https://ifp.hal.science/hal-03619397>**

Submitted on 25 Mar 2022

**HAL** is a multi-disciplinary open access archive for the deposit and dissemination of scientific research documents, whether they are published or not. The documents may come from teaching and research institutions in France or abroad, or from public or private research centers.

L'archive ouverte pluridisciplinaire **HAL**, est destinée au dépôt et à la diffusion de documents scientifiques de niveau recherche, publiés ou non, émanant des établissements d'enseignement et de recherche français ou étrangers, des laboratoires publics ou privés.

1  
2  
3  
4  
5  
6  
7  
8  
9 Impact of adsorption kinetics on pollutant dispersion in  
10 water flowing in nanopores: A Lattice Boltzmann  
11 approach to stationary and transient conditions  
12  
13  
14

15 Zaineb Zaafour

16 *IFP Energies Nouvelles, 1 & 4 Av. Bois Préau, 92852 Rueil Malmaison, France*

17 *Université Grenoble Alpes, CNRS, LIPhy, 38000 Grenoble, France*

18  
19  
20  
21 Guillaume Batôt

22 *IFP Energies Nouvelles, 1 & 4 Av. Bois Préau, 92852 Rueil Malmaison, France*

23  
24  
25 Carlos Nieto-Draghi

26 *IFP Energies Nouvelles, 1 & 4 Av. Bois Préau, 92852 Rueil Malmaison, France*

27  
28  
29 Benoit Coasne

30 *Université Grenoble Alpes, CNRS, LIPhy, 38000 Grenoble, France*

31  
32 Daniela Bauer

33 *IFP Energies Nouvelles, 1 & 4 Av. Bois Préau, 92852 Rueil Malmaison, France*  
34  
35  
36  
37  
38  
39

---

40 **Abstract**

41 We investigate the strong impact of adsorption thermodynamics and kinet-  
42 ics on particle dispersion using a robust numerical scheme: Lattice Boltz-  
43 mann simulation within the two relaxation time framework. By modeling  
44 the transport of both non-adsorbing and adsorbing molecules in simple pore  
45 structures, we highlight the key role played by the adsorption/desorption ra-  
46 tio  $k$  and the initial concentration  $c_0$  (for different adsorption models Henry,  
47 Langmuir, etc.). Considering small  $k$  or  $c_0$  leads to small or negligible adsorp-  
48 tion impact on transport. However, for larger values, adsorption significantly  
49  
50  
51  
52

53  
54 \*corresponding authors

55 *Email addresses:* benoit.coasne@univ-grenoble-alpes.fr (Benoit Coasne),  
56 daniela.bauer@ifpen.fr (Daniela Bauer)  
57  
58  
59  
60  
61  
62  
63  
64  
65

1  
2  
3  
4  
5  
6  
7  
8  
9  
10  
11  
12  
13  
14  
15  
16  
17  
18  
19  
20  
21  
22  
23  
24  
25  
26  
27  
28  
29  
30  
31  
32  
33  
34  
35  
36  
37  
38  
39  
40  
41  
42  
43  
44  
45  
46  
47  
48  
49  
50  
51  
52  
53  
54  
55  
56  
57  
58  
59  
60  
61  
62  
63  
64  
65

alters transport as it drastically increases the dispersion of the adsorbing particles within the confining geometry. Our results highlight the need to include a robust thermodynamic modeling framework in transport equations when considering complex pollutants as they display a rich and complex physicochemical behavior. This includes surfactants, which are at the core of the present work, but also molecules of emerging concern such as heavy metals, microplastics, pharmaceuticals, etc. As illustrated here, with complex interfacial effects, large deviations can be observed in both the predicted adsorbed amounts and transport dispersion coefficients when compared to molecules with more conventional adsorption properties.

*Keywords:* dispersion, adsorption, kinetics, transient regime, cooperative adsorption, Lattice Boltzmann, TRT

---

## 1. Introduction

Transport in a porous medium is relevant to a large body of domains and applications such as reservoir engineering (e.g. hydrocarbon transport in rocks), geoscience (e.g. pollutant transport in soil, radioactive waste storage in the underground), construction engineering (e.g. moisture transport control), hydrogeology (e.g. water circulation in aquifers, contaminant dispersion at the subsurface, water treatment), etc. Other applications are relevant to chemistry and physical chemistry such as in catalysis and chromatography but also in less expected fields such as bio/nanomedicine (e.g. drug delivery using encapsulating media). Fluid transport in porous media (i.e. carrier fluids) and mass transport (i.e. pollutants Bear and Cheng (2010), surfactants Kwok et al. (1993, 1995)) through flowing fluids such as water, oil and air are often impacted by different phenomena such as adsorption and chemical reactions (Rolle and Le Borgne (2019)). For purification applications, in particular, understanding the transport of pollutants inside different porous media remains a complex task as pollutants can adsorb to the solid surface following specific underlying adsorption kinetics (Manoranjan and Stauffer (1996); Appadu (2016)). If these adsorbates are in contact long enough with the adsorbent, a local equilibrium is reached between the adsorbed molecules and the molecules transported in solution. Understanding such coupling between transport and adsorption kinetics is part of many research projects (Bear (2018); Wu and Zhang (2016); Ichikawa and Selvadurai (2012); Coasne (2016); Roque-Malherbe (2018); Levesque et al. (2012, 2013);

1  
2  
3  
4  
5  
6  
7  
8  
9 Vanson et al. (2015, 2017b,a)) but further understanding, especially in the  
10 case of more complex molecules, is crucially needed to develop and improve  
11 a large number of processes belonging to different domains. Regardless of  
12 the field and application envisaged, rationalizing transport in porous media  
13 requires to better describe the link between the descriptors that character-  
14 ize porous media and the fluid flow mechanisms including adsorption within  
15 their porosity.  
16

17  
18 Beyond pioneering works, particular attention should be paid to the spec-  
19 ific adsorption behavior of complex pollutants. In particular, surfactants  
20 – which are used to clean natural water polluted during oil extraction or  
21 to depollute industrial sites containing hydrocarbons – are a non-negligible  
22 water pollution source that leads to complex water treatment challenges.  
23 Among other complex compounds, micropollutants – which are the subject  
24 of increasing attention worldwide – include microplastics (Eerkes-Medrano  
25 et al. (2015); Petersen and Hubbart (2021)), metals, organic/pharmaceutical  
26 molecules, and persistent personal care pollutants. All these systems have in  
27 common with surfactants to follow physico-chemical behaviors that cannot  
28 be described using classical adsorption models (Henry, Langmuir) (Wolanin  
29 et al. (2020, 2021)). In particular, they are characterized by aggregation  
30 effects and the ability to form structures at interfaces which strongly differ  
31 from their volumetric behavior. Without being fully understood, this specific  
32 interfacial behavior is known to influence the transport properties of these  
33 molecule types. In this work, by focussing on the coupling between trans-  
34 port and adsorption, we illustrate the importance of including this rich and  
35 complex behavior – which cannot be predicted by conventional approaches –  
36 in transport equations.  
37

38  
39 In porous media, upon adding solutes (e.g. surfactants, pollutants) to a  
40 flowing solvent (e.g. water), the former tend to disperse in the solid porosity.  
41 Dispersion is the phenomenon that results from the combination of advection  
42 and diffusion in porous media (Sahimi (2012)). Typically, after injection, in  
43 the long time limit, solute particles in the flowing fluid will be dispersed  
44 homogeneously. Therefore, understanding the time dependence of particle  
45 distributions provides a mean to better design engineering processes (and  
46 particularly groundwater remediation). Fluid flow through a porous medium  
47 can exhibit a rich behavior as a result of the complexity of the porous struc-  
48 ture. Collision with pore edges and changes in fluid pathways lead to the  
49 mixing and re-arrangement of the moving particles. Such dispersion, which  
50 manifests itself at the macroscopic level, results from the simultaneous ac-  
51  
52  
53  
54  
55  
56

tion of mechanical and macroscopic phenomena (Fried (1975); Payne et al. (2008)). On the one hand, mechanical dispersion results from the fact that the fluid is moving at both higher and lower velocities than the mean velocity (Fetter (1994)). In particular, the flowing fluid in the porous medium follows preferential pathways as its transport through small pores is slower than through large pores. As a result, since particles do not move at the same velocity everywhere, significant dispersion is observed along the flow paths. In turn, such dispersion leads to a broad distribution of solute particles at the flow edge. On the other hand, macroscopic dispersion corresponds to the spreading of solute particles caused by the heterogeneity at the porous medium scale (i.e. well beyond the pore scale). Such heterogeneity causes variations in the local permeability that lead to heterogeneous flows with significant spatial variations in the advective velocity field. In summary, dispersion in porous media is driven by physical parameters characterizing the transport properties of the complex fluid system but also by the main descriptors related to the host porous medium. These parameters include the molecular diffusion coefficient of the particles, the Stokes velocity field of the flowing fluid, the kinematic and rheological properties of the fluid (*in situ* viscosity, shear effect of the flow), and the geometry of the porous medium (in particular, its porosity and its characteristic interstitial length).

In conclusion, passive tracer transport in porous media is a complex phenomenon and still subject of ongoing research. To disentangle the effects of pore structure from those due to a rich adsorption behavior, as it is for example the case of pollutants, we perform transport simulations of adsorbing molecules in simple pore channels. Of particular relevance to practical situations, using an original numerical strategy, transient regimes are thoroughly investigated using such a simple pore geometry. Their understanding is particularly important for transport in porous media as the effective Taylor regime is rarely reached in porous structures. Understanding transport of these types of molecules in simplified structures allows gaining insights into the coupling between transport and particular adsorption kinetics.

Considering transport processes involving advection, diffusion and adsorption phenomena, the mass conservation of the solutes transported by the flow in porous media can be described by the so-called advection–diffusion–adsorption equation (ADA) (Kwok et al. (1995)):

$$\frac{\partial c}{\partial t} + \mathbf{U} \cdot \nabla c - \nabla \cdot (D \nabla c) + \frac{1 - \phi}{\phi} \frac{\partial \Gamma}{\partial t} = 0 \quad (1)$$

1  
 2  
 3  
 4  
 5  
 6  
 7  
 8  
 9 where  $c$  is the concentration of the adsorbing solutes in the liquid phase,  $\Gamma$  is the amount of adsorbed solutes,  $\phi$  is the average porosity,  $\mathbf{U}$  is the velocity vector, and  $D$  is the dispersion tensor.  $\Gamma$  is related to the concentration  $c$  in the liquid phase under equilibrium and non-equilibrium conditions following an underlying adsorption kinetics. In the present work, we are interested in the modeling of solute adsorption under dynamic conditions – i.e. under flow conditions. Despite considering transport and adsorption of surfactants, we emphasize that the results reported in this contribution can be extended well-beyond this specific system. In particular, we aim at considering how flow/transport couple with adsorption kinetics with key questions to be answered regarding the impact on particle dispersion of “wall effects” (i.e. adsorption/desorption phenomena, surface diffusion, etc. (Berezhkovskii and Skvortsov (2013))). Particularly, understanding the coupling in complex porous media between the porous medium structure and adsorption kinetics still requires further understanding (Coasne et al. (2013); Galarneau et al. (2016); Boğan et al. (2015))). With this goal, we use the Lattice Boltzmann Method (LBM) as recently developed in our group to integrate adsorption kinetics into transport models and to consider different mechanisms involved (mass transfer, diffusion, and adsorption) (Zaafouri et al. (2021)). LBM, which has already been used to simulate complex physical phenomena in porous media (among many others Gray et al. (2016); Gray and Boek (2016); Boek et al. (2017)) and particularly adsorption processes (Xu et al. (2018, 2019); Ning et al. (2015); Sukop and Or (2004); Agarwal et al. (2005); Manjhi et al. (2006); Asta et al. (2018); Vanson et al. (2015, 2017b,a); Levesque et al. (2013)), was shown to be an efficient and robust numerical method to simulate miscible transport of adsorbing molecules with different adsorption kinetics (Zaafouri et al. (2021)). In practice, our numerical method relies on the Two Relaxation Time scheme (Batôt et al. (2016); Ginzburg et al. (2010); Talon et al. (2012)).

10  
 11  
 12  
 13  
 14  
 15  
 16  
 17  
 18  
 19  
 20  
 21  
 22  
 23  
 24  
 25  
 26  
 27  
 28  
 29  
 30  
 31  
 32  
 33  
 34  
 35  
 36  
 37  
 38  
 39  
 40  
 41  
 42  
 43  
 44  
 45  
 46 A simple channel geometry consisting of two parallel plates is used to simulate the dispersion of either non-adsorbing or adsorbing tracers (i.e. solutes). This geometry having dimensions  $L_x \times L$  is shown in Fig. 1(a) where the white sites correspond to bulk-like regions of the system and the black sites correspond to solid sites. In the LBM simulations, our geometry is exposed to a fluid flow that obeys a Stokes flow  $\mathbf{U}$  with an average flow rate  $U$ . The Peclet number, which characterizes the ratio of advection/diffusion phenomena, is defined as  $Pe = UL/D_m$  where we recall that  $D_m$  is the solute molecular diffusion coefficient. At a time  $t = 0$ , the tracer particles are in-

1  
 2  
 3  
 4  
 5  
 6  
 7  
 8  
 9  
 10  
 11  
 12  
 13  
 14  
 15  
 16  
 17  
 18  
 19  
 20  
 21  
 22  
 23  
 24  
 25  
 26  
 27  
 28  
 29  
 30  
 31  
 32  
 33  
 34  
 35  
 36  
 37  
 38  
 39  
 40  
 41  
 42  
 43  
 44  
 45  
 46  
 47  
 48  
 49  
 50  
 51  
 52  
 53  
 54  
 55  
 56  
 57  
 58  
 59  
 60  
 61  
 62  
 63  
 64  
 65

jected with an initial concentration  $c_0$ . Such concentration injection can be performed in several ways: (1) a concentration is injected as Dirac pulse at a specific time at a lateral position in the geometry or (2) a concentration is injected continuously for a fixed time period. These two configurations consist in defining a lateral position  $x = x_0$  in the geometry and injecting the concentration at this position for a determined period of time  $\Delta t_0 = n\Delta t$ . Thus, as illustrated in Fig. 1(b), according to the specific value of  $n$  used, the situation refers to a continuous “slug” injection ( $n > 1$ ) or a Dirac pulse injection ( $n = 1$ ). More precisely, for a position  $\mathbf{r}_0 = (x_0, y)$ , we inject tracer particles with the initial concentration  $c_0$  such that  $c(\mathbf{r}_0) = c_0$  over a period  $\Delta t_0 = n\Delta t$ . For  $n = 1$ , Fig. 1(a) schematically illustrates the tracer concentration distribution as a function of time (i.e. tracer dispersion). We evaluate the impact of adsorption on the free tracer distribution by studying the displacement variance  $\sigma^2(t)$  along the flow direction  $x$ . Its derivative allows a direct estimation of the effective dispersion coefficient  $D(t \rightarrow \infty)$  where  $D(t) \sim d\sigma^2(t)/2dt$ .

In practice, we focus on two specific issues: First, we investigate the effect of system parameters such as the initial concentration  $c_0$  and the adsorption/desorption ratio  $k$  of different adsorption models on the transport regimes. In this respect, we note that while existing works have already considered to some extent such aspects, we extend here this investigation to transient regimes. Such non stationary regimes are very important since, as already stated, many practical situations show that water and pollutants do not reach Taylor dispersion. Also, Kahlen et al. (2017) showed that the displacement distributions strongly depend on the symmetry or asymmetry of transition rates. In a second step, we focus on the cooperative adsorption of complex molecules and the resulting transport behavior. Such aspects are equally important since available works in the literature only consider simple adsorption regimes (Henry, Langmuir) which fail to describe the adsorption of complex molecules such as micropollutants.

The remaining of this paper is structured as follows. In Section 2, we introduce the different adsorption models and present the most important features of the extended Lattice Boltzmann scheme (further information can be found in the Supplemental Information). In Section 3, we describe our results for transport obtained upon Dirac pulse injection in the case of Henry and Langmuir adsorption models (different adsorption/desorption ratios  $k$  and initial concentrations  $c_0$  are considered). Then, we compare the results obtained for the different adsorption models upon continuous injection. In

1  
2  
3  
4  
5  
6  
7  
8  
9  
10  
11  
12  
13  
14  
15  
16  
17  
18  
19  
20  
21  
22  
23  
24  
25  
26  
27  
28  
29  
30  
31  
32  
33  
34  
35  
36  
37  
38  
39  
40  
41  
42  
43  
44  
45  
46  
47  
48  
49  
50  
51  
52  
53  
54  
55  
56  
57  
58  
59  
60  
61  
62  
63  
64  
65

Section 4, we summarize our findings and provide perspectives for further developments and applications.

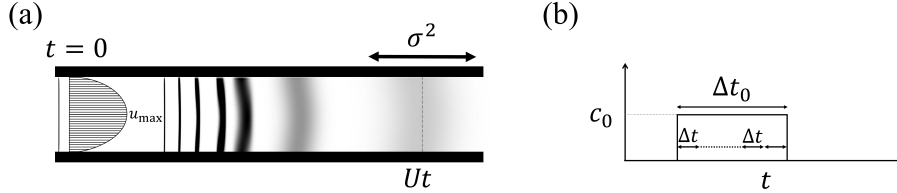


Figure 1: (a) Illustration of the dispersion phenomena for a Dirac pulse injection of solute particles at an initial concentration  $c_0$  at time  $t = 0$ . The porous material consists of two parallel plates subjected to a solvent fluid transported according to a Poiseuille flow (with mean and maximum velocities  $U$  and  $U_{max}$ , respectively). In the long time limit, the solute variance  $\sigma^2$  evolves linearly with time  $t$  with a behavior that is directly related to the dispersion coefficient  $D$ . (b) Continuous injections, referred to as “slug” injections, can be modelled by injecting a constant concentration  $c_0$  for a given period of time  $\Delta t_0 = n\Delta t$  (with  $\Delta t$  the duration of an iteration step in the Lattice Boltzmann scheme and  $n$  a chosen integer). Dirac pulse injection is obtained when setting  $n = 1$  while continuous injection over a certain period of time is obtained for  $n > 1$ . color online only

## 2. Methods

We are interested in the modeling of surfactant adsorption under dynamic (i.e. flow) conditions. For certain parameter ranges, adsorption considerably impacts the transport of these molecules. To gain further insight into the coupling between adsorption and transport of such complex molecules, we employ the Lattice Boltzmann approach introduced in (Zaafouri et al. (2021)) which allows considering different adsorption models. In more detail, we consider the following adsorption mechanisms: the Henry regime, the Langmuir regime (which accounts for surface adsorption saturation), and the cooperative model recently introduced to account for collective adsorption effects (Zaafouri et al. (2020)). In what follows, we introduce the analytical form of the underlying adsorption kinetics as well as their corresponding Lattice Boltzmann equations for these different models: Henry, Langmuir and cooperative adsorption.

### 2.1. Adsorption kinetics

**Henry model.** With this model, the adsorbed amount is assumed to be proportional to the adsorbate concentration in the bulk solution from which

adsorption occurs. The underlying kinetics leading to the so-called Henry adsorption isotherm at equilibrium corresponds to:

$$\frac{\partial \Gamma}{\partial t} = k_A c \Gamma^0 - k_D \Gamma \quad (2)$$

where  $k_A$  and  $k_D$  are the adsorption and the desorption rates while  $\Gamma^0$  represents a characteristic adsorbed amount. The solution resulting from Henry adsorption kinetics in Eq. 2 is given by:

$$\Gamma(t) = \Gamma^0 [1 - e^{-k_D t}] k_H c \quad (3)$$

with  $k_H = k_A/k_D$  which results in the following adsorption isotherm:  $\Gamma(t) = \Gamma^0 k_H c$ .

**Langmuir model.** With this model, it is assumed that the molecules are adsorbed on well-defined sites at the adsorbent surface. All sites are considered identical and only one molecule can be adsorbed in each site (therefore, leading to monomolecular layers only). Such surface saturation is characteristic of Langmuir adsorption. The dynamical equilibrium between the molecules that are adsorbed at the surface and those that desorb from the surface is described by the following kinetic equation:

$$\frac{\partial \Gamma}{\partial t} = k_A c (\Gamma^\infty - \Gamma) - k_D \Gamma \quad (4)$$

where  $\Gamma^\infty$  represents the adsorbed amount at surface saturation. The solution resulting from the Langmuir kinetics in Eq. 4 is given by:

$$\Gamma(t) = [1 - e^{-k_D(1+k_L c)t}] \frac{\Gamma^\infty k_L c}{1 + k_L c} \quad (5)$$

where  $k_L = k_A/k_D$ . At equilibrium (i.e. in the limit of infinite time), the adsorption isotherm becomes  $\Gamma(t) = \Gamma^\infty k_L c / [1 + k_L c]$ .

**Cooperative model.** This thermodynamic model captures the collective adsorption behavior of surfactants (or any other molecules with strong cooperative effects) leading to complex kinetics and structural (re)arrangement upon adsorption. Full details on this recent model can be found in (Zaafouri et al. (2020)) so that only key elements will be presented here. We introduce a surface critical concentration  $c_s$  below which only adsorption of individual monomers  $m$  occurs; in this concentration range, adsorption follows either the Henry or the Langmuir model. Above  $c_s$ , both individual monomers  $m$

and aggregated monomers  $m'$  get adsorbed at the surface sites  $s$ . As shown in (Zaafouri et al. (2020)), the underlying kinetics for the adsorption of aggregated monomers writes:

$$\frac{\partial \Gamma_{m'}(c, t)}{\partial t} = k'_A(\Gamma_{m'})c[\Gamma^\infty - \Gamma_m(c, \infty) - \beta \Gamma_{m'}(c, t)] - k'_D(\Gamma_{m'})\Gamma_{m'}(c, t) \quad (6)$$

where  $\Gamma_{m'}(c, t)$  is the surface concentration of aggregated monomers  $m'$  and  $\Gamma_m(c, \infty)$  is the surface concentration of individually adsorbed monomers  $m$ .  $\beta$  presents the fraction of the solid sites occupied by the aggregated monomers. The parameters  $k'_A(\Gamma_{m'})$  and  $k'_D(\Gamma_{m'})$  are the adsorption and desorption rates depending on the actual surface concentration  $\Gamma_{m'}$ . The solution of this kinetic equation for a bulk concentration  $c$  is given by:

$$\Gamma_{m'}(c, \infty) = [\Gamma^\infty - \Gamma_m(c, \infty)] \frac{k'(\Gamma_{m'})c}{[1 + \beta ck'(\Gamma_{m'})]} \quad (7)$$

where  $k'(\Gamma_{m'}) = k'_A(\Gamma_{m'})/k'_D(\Gamma_{m'})$ .

Fig. 2 shows the experimental adsorption isotherm for surfactant (TX100) on silica taken from (Denoyel and Rouquerol (1991)) as well as the Henry, Langmuir and Cooperative Langmuir adsorption isotherms which allow decomposing such adsorption data into individual and aggregated monomers (for more detail, see (Zaafouri et al. (2020))). The model parameters are given in the caption of Fig. 2. On the one hand, for the Langmuir model,  $k_L$  provides the best fit of the experimental data above  $c_s$ . On the other hand,  $k_H$  was obtained by fitting the experimental data for  $c < c_s$ . Data of  $k'(\Gamma_{m'})$  is provided in the Supplemental Information (Fig. S1).

## 2.2. Lattice Boltzmann

Before introducing the technical details at the core of our Lattice Boltzmann scheme, we present a quick state of the art on such methods applied to adsorption and transport in porous media. Among other methods (e.g. Appadu (2016); Asta et al. (2018); Hlushkou et al. (2014)), Lattice Boltzmann schemes are very suitable for this type of computation as they are highly parallelizable. Indeed, the investigation of transient and stationary transport regimes requires relatively large simulations in time and space. Guo et al. (2016) applied a Lattice Boltzmann scheme to simulate adsorption characterized by different isotherms. Likewise, Xu et al. (2018, 2019) used a Lattice Boltzmann method to simulate gas adsorption in nanopores of shale.

1  
2  
3  
4  
5  
6  
7  
8  
9  
10  
11  
12  
13  
14  
15  
16  
17  
18  
19  
20  
21  
22  
23  
24  
25  
26  
27  
28  
29  
30  
31  
32  
33  
34  
35  
36  
37  
38  
39  
40  
41  
42  
43  
44  
45  
46  
47  
48  
49  
50  
51  
52  
53  
54  
55  
56  
57  
58  
59  
60  
61  
62  
63  
64  
65

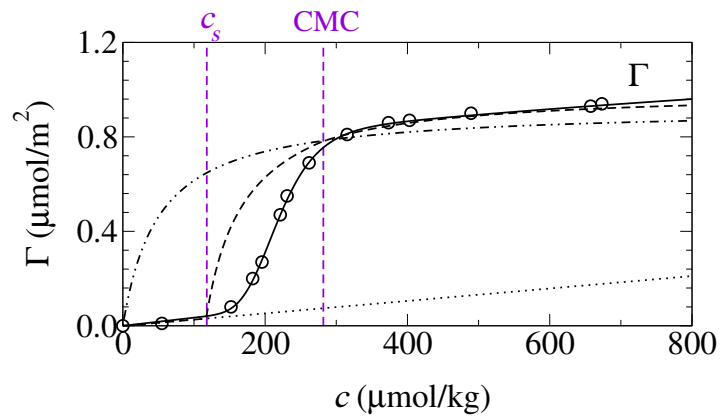


Figure 2: Adsorption isotherm for aggregated monomers showing the surface concentration of surfactants  $\Gamma$  onto a silica-based surface as a function of the bulk concentration  $c$ . The black symbols are the experimental data taken from (Denoyel and Rouquerol (1991)) with the black line corresponding to the fit using the cooperative adsorption model. The dotted line denotes the Henry isotherm with  $k_H = 2.6 \times 10^{-6}$  which describes the adsorption of individual monomers in the region  $c < c_s$ . The dash-dotted line corresponds to the Langmuir model with  $k_L = 0.026$  and  $\Gamma^\infty = 0.92$ . The dashed line denotes the Henry-Langmuir model with  $k_L$  and  $k_H$  as the Langmuir and Henry constants, respectively. In all these data,  $c_s = 117 \mu\text{mol/kg}$  and  $\text{CMC} = 281.81 \mu\text{mol/kg}$ . color online only

1  
2  
3  
4  
5  
6  
7  
8  
9  
10  
11  
12  
13  
14  
15  
16  
17  
18  
19  
20  
21  
22  
23  
24  
25  
26  
27  
28  
29  
30  
31  
32  
33  
34  
35  
36  
37  
38  
39  
40  
41  
42  
43  
44  
45  
46  
47  
48  
49  
50  
51  
52  
53  
54  
55  
56  
57  
58  
59  
60  
61  
62  
63  
64  
65

However, the latter studies only consider adsorption phenomena of particles transported by pure diffusion. Ning et al. (2015) used a Multiple Relaxation Time Lattice Boltzmann scheme extended to adsorption phenomena to simulate gas flow in nanopores. They were particularly interested in the joint effect of adsorption and gas slippage on gas flow. Interactions between the adsorbate and the surface were modelled by the so-called adsorptive force (Sukop and Or (2004)). Agarwal et al. (2005) and Manjhi et al. (2006) also investigated the coupling between adsorption and transport in a flowing fluid by considering first order adsorption kinetics. Simulations were only performed in the Henry regime, characterized by the proportionality of the bulk concentration and the adsorbed quantity, and consequently at low concentrations. Manjhi et al. (2006) used a constant dispersion coefficient in their Lattice Boltzmann method, making the investigation of the effect of adsorption on the different transport regimes difficult. Further on, Rotenberg and coworkers (Levesque et al. (2013); Vanson et al. (2015); Asta et al. (2018)) proposed an extended Lattice Boltzmann scheme allowing the investigation of the adsorption impact on the behavior of solutes and solvent under flow conditions. Here, adsorption takes place in fluid nodes in direct contact with the nodes of the solid interface. They define free and adsorbed concentrations/quantities to determine equilibrium properties after each simulation/adsorption step. Their transport computations are based on the moment propagation method (Ladd and Verberg (2001); Merks et al. (2002)), and they introduced propagators for the adsorbed and free concentrations. Dynamic properties of solute dispersion in a flowing fluid can be determined in this way. Rotenberg and coworkers were particularly interested in the coupling between adsorption and fluid flow in the stationary, long time limit regime, once that the thermodynamic equilibrium is attained. Nevertheless, further understanding of transient regimes, where the timescale of adsorption might be comparable to the one of dispersion remains crucial, particularly in the case of transport in porous media. To this goal, Vanson et al. (2017a,b) extended the numerical scheme proposed by Levesque et al. (2013). Their method now includes Langmuir kinetics and allows the simulation of the interplay between adsorption and transport in a kinetics regime. However, Vanson et al. don't perform a thorough investigation of the effect of adsorption and system parameters on the transient dispersion regimes. Also, adsorption kinetics of complex molecules such as pollutants are not included in their extended Lattice Boltzmann approach. Consequently as mentioned above, we focus in this article on two specific subjects: the influence of system

1  
2  
3  
4  
5  
6  
7  
8  
9 parameters on the transient regimes and the transport of complex molecules  
10 following cooperative adsorption.

11 We use a novel Lattice Boltzmann scheme which enables us to reproduce  
12 the thermodynamics and kinetics of adsorption; this efficient numerical tech-  
13 nique was shown to provide results in very good agreement with analytical  
14 solutions (Levesque et al. (2012)). Detailed validation steps can be found in  
15 Zaafour et al. (2021). In this article, we consider in detail the influence of  
16 different adsorption models and their parameters on the interplay between  
17 adsorption and transport in porous media. In short, our Lattice Boltzmann  
18 simulations involve different steps. After specification of the pore geometry,  
19 we first compute Stokes flow of the carrier fluid by means of an independ-  
20 ent Lattice Boltzmann simulation. In a second step, we perform transport  
21 simulations of adsorbing molecules. In what follows, we detail the compu-  
22 tational aspects of the adsorption kinetics of tracer molecules coupled to  
23 their transport. For further information on the standard Lattice Boltzmann  
24 schemes to solve Stokes equation and Advection-Diffusion equation (includ-  
25 ing the implementation of boundary conditions), the reader is referred to  
26 the Supplemental Information file. Here, we focus the content of this meth-  
27 ods section on the main novel technical ingredients which allow including  
28 adsorption thermodynamics and kinetics.

29 Tracers are injected at the beginning of the transport simulation at a spe-  
30 cific time  $t = 0$  as presented in Fig. 1. Considering these initial conditions,  
31 we then proceed to the calculation of the adsorption kinetics and transport  
32 of the tracer molecules. At each time step  $\Delta t$ , we perform consecutively  
33 the following intermediate steps: collision, adsorption, and propagation to  
34 redistribute the free and adsorbed tracers (See Fig. S1 in the Supplemental  
35 Information). The system is characterized by the free and adsorbed tracer  
36 concentrations respectively:  $c(\mathbf{r}, t)$  and  $c_a(\mathbf{r}, t)$ . This means, that if there is  
37 a solid/fluid interface at position  $\mathbf{r}$ , the adsorbed quantity in this position  
38 corresponds to  $c_a(\mathbf{r}, t)$ . In practice, the free tracer concentration is related to  
39 the distribution  $g_q(\mathbf{r}, t)$  which corresponds to the free tracer density having  
40 a velocity  $\mathbf{v}_q$  along the direction  $q$  at time  $t$  and position  $\mathbf{r}$ . In all our sim-  
41 ulations, we use the D2Q9 scheme classification whose velocity set includes  
42 four “coordinate” velocities  $\mathbf{v}_q = (\pm 1, 0), (0, \pm 1)$ , four “diagonal” velocities  
43  $\mathbf{v}_q = (\pm 1, \pm 1)$  and the immobile (zero velocity). Throughout this document,  
44 these velocity components are denoted  $\mathbf{v}_q$  (with  $q \in \{0, \dots, q_m = 8\}$ ). The  
45 concentration is linked to the density distribution as  $c(\mathbf{r}, t) = \sum_q g_q(\mathbf{r}, t)$ .

We define the symbols  $\tilde{\cdot}$  and  $\tilde{\cdot}$  to refer to quantities obtained after the intermediate collision and adsorption steps. Consequently,  $\tilde{c}(\mathbf{r}, t) = \sum_q \tilde{g}_q(\mathbf{r}, t)$ ,  $\tilde{\tilde{c}}(\mathbf{r}, t) = \sum_q \tilde{\tilde{g}}_q(\mathbf{r}, t)$ , and  $c(\mathbf{r}, t) = \sum_q g_q(\mathbf{r}, t)$  correspond to the free tracer concentrations obtained after the collision, adsorption and propagation steps, respectively. The collision and propagation steps are identical to those used for conventional Lattice Boltzmann simulations with the Two Relaxation Time scheme to solve the advection/diffusion equation. As described in the SI file, free particles follow the classical bounce back boundary condition at the solid-liquid interface corresponding to a no-slip condition. In what follows, we will only consider the features related to the adsorption step as it depends on the specific adsorption kinetics under study.

The adsorption step obeys the first order kinetic equation leading to the adsorption isotherm at equilibrium. In the present work, as already stated, we consider Henry, Langmuir, and cooperative adsorption models. When performing the adsorption step, for a given adsorption model,  $c(\mathbf{r}, t)$  and  $c_a(\mathbf{r}, t)$  vary according to the underlying kinetics equation. In practice, from the free and adsorbed tracer concentrations [ $\tilde{c}(\mathbf{r}, t)$  and  $\tilde{c}_a(\mathbf{r}, t)$ ] computed at time  $t$  after the collision step, the adsorption step yields updated concentrations  $\tilde{\tilde{c}}(\mathbf{r}, t)$  and  $\tilde{\tilde{c}}_a(\mathbf{r}, t)$ . In what follows, we provide the kinetic equations for the different adsorption models considered in this work.

**Henry adsorption.** The Lattice Boltzmann adsorption kinetics for Henry adsorption can be written as:

$$\tilde{\tilde{c}}_a(\mathbf{r}, t) = p_A \tilde{c}(\mathbf{r}, t) + [1 - p_D] \tilde{c}_a(\mathbf{r}, t) \quad (8)$$

$$\tilde{\tilde{c}}(\mathbf{r}, t) = \tilde{c}(\mathbf{r}, t) - p_A \tilde{c}(\mathbf{r}, t) + p_D \tilde{c}_a(\mathbf{r}, t) \quad (9)$$

with  $p_A$  and  $p_D$  being the adsorption and desorption rates given in Lattice Boltzmann units. Values for  $p_A$  and  $p_D$  are obtained by mapping the above equation with the physical kinetic equation:  $p_A = k_A \Delta t / \Delta x$  and  $p_D = k_D \Delta t$ .

**Langmuir adsorption.** The Langmuir adsorption model considers surface saturation as adsorption proceeds. This implies that the adsorbed concentration  $c_a(\mathbf{r}, t)$  is always lower than a characteristic surface concentration  $c_a^\infty$ . In this case, Eqs. 8 and 9 are modified to take surface saturation into account:

$$\tilde{\tilde{c}}_a(\mathbf{r}, t) = p_A \tilde{c}(\mathbf{r}, t) \left[ 1 - \frac{\tilde{c}_a(\mathbf{r}, t)}{c_a^\infty} \right] + (1 - p_D) \tilde{c}_a(\mathbf{r}, t) \quad (10)$$

$$\tilde{c}(\mathbf{r}, t) = \tilde{c}(\mathbf{r}, t) - p_A \tilde{c}(\mathbf{r}, t) \left[ 1 - \frac{\tilde{c}_a(\mathbf{r}, t)}{c_a^\infty} \right] + p_D \tilde{c}_a(\mathbf{r}, t) \quad (11)$$

Here, the maximum surface concentration can be written as  $\Gamma^\infty = c_a^\infty \Delta x$  with  $p_A$  and  $p_D$  defined as for the Henry model:  $p_A = k_A \Delta t / \Delta x$  and  $p_D = k_D \Delta t$ .

**Cooperative adsorption.** This advanced model, which allows considering the adsorption of complex molecules leading to collective surface effects, considers two different adsorbed concentrations: the concentration of adsorbed isolated monomers  $c_{a,m}(\mathbf{r}, t)$  and the concentration of adsorbed aggregated monomers  $c_{a,m'}(\mathbf{r}, t)$ . The overall surface concentration is then obtained by summing these two quantities:  $c_a(\mathbf{r}, t) = c_{a,m}(\mathbf{r}, t) + c_{a,m'}(\mathbf{r}, t)$ . Furthermore, we assume that the adsorption of isolated monomers is instantaneous compared to that of aggregated monomers:  $c_{a,m}(\mathbf{r}, t) = c_{a,m}(\mathbf{r}, \infty) \forall t$ . This cooperative model can be implemented in the Lattice Boltzmann scheme by modifying Eqs. 8 and 9:

$$\tilde{c}_{a,m'}(\mathbf{r}, t) = p'_A \tilde{c}(\mathbf{r}, t) \left[ 1 - \frac{\beta \tilde{c}_{a,m'}(\mathbf{r}, t) + c_{a,m}(\mathbf{r}, \infty)}{c_a^\infty} \right] + (1 - p'_D) \tilde{c}_{a,m'}(\mathbf{r}, t) \quad (12)$$

$$\tilde{c}(\mathbf{r}, t) = \tilde{c}(\mathbf{r}, t) - p'_A \tilde{c}(\mathbf{r}, t) \left[ 1 - \frac{\beta \tilde{c}_{a,m'}(\mathbf{r}, t) + c_{a,m}(\mathbf{r}, \infty)}{c_a^\infty} \right] + p'_D \tilde{c}_{a,m'}(\mathbf{r}, t) \quad (13)$$

where  $c_a^\infty = \Gamma^\infty / \Delta x$ ,  $p'_A = k'_A \Delta t / \Delta x$  and  $p'_D = k'_D \Delta t$  and  $\Gamma_{m'}(\mathbf{r}, t) = c_{a,m'}(\mathbf{r}, t) \Delta x$ . During the adsorption step, unlike for the propagation and collision steps, the fraction  $\tilde{x}_q(\mathbf{r}, t) = \tilde{g}_q(\mathbf{r}, t) / \tilde{c}(\mathbf{r}, t)$  remains constant [i.e.  $\tilde{x}_q(\mathbf{r}, t) = \tilde{\tilde{x}}_q(\mathbf{r}, t)$ ].  $\tilde{\tilde{x}}_q(\mathbf{r}, t) = \tilde{g}_q(\mathbf{r}, t) / \tilde{c}(\mathbf{r}, t)$  is the fraction of particles belonging to a velocity set  $\mathbf{v}_q$  at position  $\mathbf{r}$  and time  $t$ . Based on the definition mentioned above, i.e.  $\tilde{c}(\mathbf{r}, t) = \sum_q \tilde{\tilde{g}}_q(\mathbf{r}, t)$ , the variation between the different  $\tilde{\tilde{g}}_q$  components caused by the adsorption operator

$$A(\tilde{c}, \tilde{c}_a) = \Delta c(\mathbf{r}, t) = \tilde{\tilde{c}}(\mathbf{r}, t) - \tilde{c}(\mathbf{r}, t) \quad (14)$$

is redistributed in a proportional and homogeneous way. This means that the molecule distributions  $\tilde{\tilde{g}}_q(\mathbf{r}, t)$  after the adsorption step are given by:

$$\tilde{\tilde{g}}_q(\mathbf{r}, t) = \tilde{g}_q(\mathbf{r}, t) - \tilde{x}_q(\mathbf{r}, t) A(\tilde{c}, \tilde{c}_a) \quad (15)$$

All details can be found in (Zaafouri et al. (2021)).

### 3. Results

The present section is organized as follows. By considering the injection of a Dirac pulse of tracer molecules, we will first compare the effect on transport phenomena of molecules adsorbing according to Henry and Langmuir models. We will also treat more specific cases by considering large adsorption constants  $k_H$  (Henry adsorption) and large initial concentrations  $c_0$  (Langmuir adsorption). Finally, we will focus on continuous i.e. “slug” injection in combination with the different adsorption models.

#### 3.1. Henry and Langmuir adsorption

Adsorption and transport can be studied by monitoring the time evolution of the concentration fields and of the displacement distributions of the tracer molecules (the so-called propagators). Moreover, the displacement variance  $\sigma_x^2(t)$  along the flow direction  $x$  allows gaining further information as it provides a direct measurement of the dispersion coefficient  $D(t) = d\sigma_x^2(t)/2dt$ . The displacement variance scales as  $\sigma_x^2(t) \propto t^\beta$ . The scaling exponent  $\beta$  is equal to one in the case of Gaussian transport and  $\beta \neq 1$  in the transient regimes.

As shown in (Zaafouri et al. (2021)), Henry adsorbing and non-adsorbing molecules, that are transported in a channel successively follow the same three transport regimes: molecular diffusion, advection-dominated transport, and Taylor dispersion. Equivalent results can be observed for molecules adsorbing according to the Langmuir model. Fig. 3 provides the concentration profiles for the Henry and Langmuir model whereas Fig. 4 shows the corresponding propagators at different times  $t$ . For both models, the propagators have a Gaussian shape for small  $t$  and large  $t$  corresponding, respectively, to the molecular diffusion and Taylor dispersion regime. Owing to adsorption, the normalized average displacement in the Taylor regime is smaller than the normalized mean fluid displacement  $[(x - x_0)/Ut < 1$  where  $U$  is the mean fluid velocity] and decreases with time  $t$ . In the intermediate advection dominated regime ( $t_2$ ), the propagators display a non-Gaussian shape with a higher probability for larger velocities. While molecules following Henry adsorption reach rapidly the Taylor regime, Langmuir adsorbing molecules require more time to attain the asymptotic state ( $t_3$ ). This can also be seen in Fig. 5 where the normalized dispersion coefficient  $D(t)/D_m$  for the Langmuir adsorbing molecules reaches a plateau at larger times (corresponding to Taylor dispersion). We computed the scaling exponent  $\beta$  for both data

1  
2  
3  
4  
5  
6  
7  
8  
9  
10  
11  
12  
13  
14  
15  
16  
17  
18  
19  
20  
21  
22  
23  
24  
25  
26  
27  
28  
29  
30  
31  
32  
33  
34  
35  
36  
37  
38  
39  
40  
41  
42  
43  
44  
45  
46  
47  
48  
49  
50  
51  
52  
53  
54  
55  
56  
57  
58  
59  
60  
61  
62  
63  
64  
65

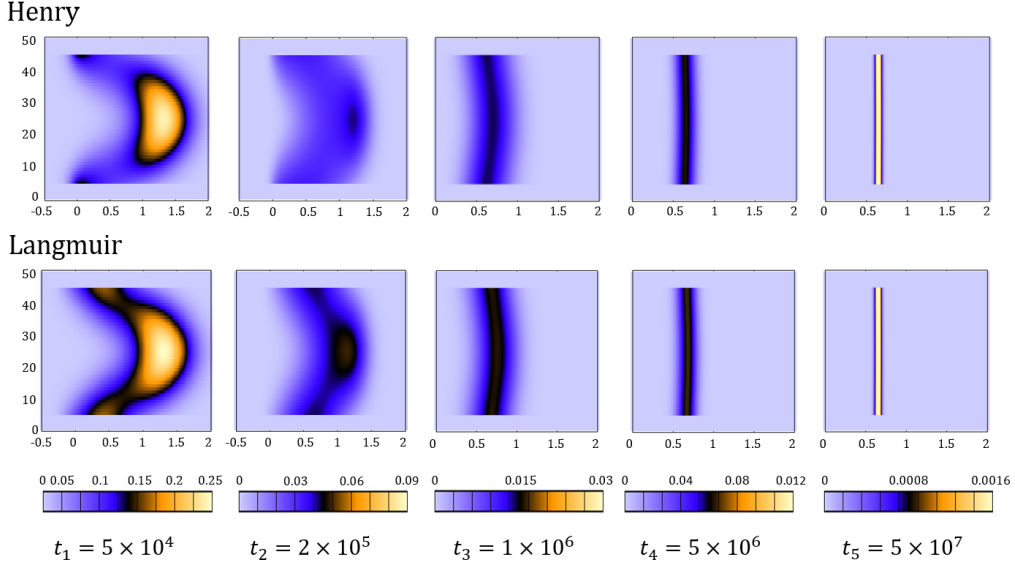


Figure 3: Concentration fields observed at different times  $t_n$ . The abscissas are plotted in units of  $(x-x_0)/Ut$  where  $x_0$  is the injection position and  $U$  the average fluid velocity. The results correspond to the dispersion of molecules obeying Henry and Langmuir adsorption isotherms (with  $k_H = k_L = 10$  and  $\Gamma^\infty = 1$ ). The Peclet number is  $Pe = 25$  and the initial concentration  $c_0 = 10$ . color online only

sets of Fig. 5. As can be already deduced from the existence of a plateau,  $\beta$  is equal to one in the long-time limit. In the intermediate transient regime, it becomes  $\beta = 1.75$  for the Henry adsorbing molecules and  $\beta = 1.58$  in the case of Langmuir adsorption. In this regime, advection dominates and the displacement variance evolves faster than in the Taylor regime.

### 3.2. Influence of $k = k_A/k_D$

Levesque et al. (2012) provided an analytical solution for the effective dispersion coefficient  $D_{eff}^{ads}/D_m$  in the case of Taylor dispersion of molecules adsorbing according to Henry adsorption.  $D_{eff}^{ads}/D_m$  is defined as the long time limit of  $D(t)/D_m$  (see Supplemental Information for more details). At this stage, to our knowledge, no analytical solution for Taylor dispersion in case of Langmuir adsorbing molecules is available. Fig. 6 shows  $D(t)/D_m$  as predicted using our numerical approach for different adsorption ratios  $k$  (both data for Henry and Langmuir adsorption are shown). In all cases,  $D(t)/D_m$  reaches a plateau in the long time limit which corresponds to the

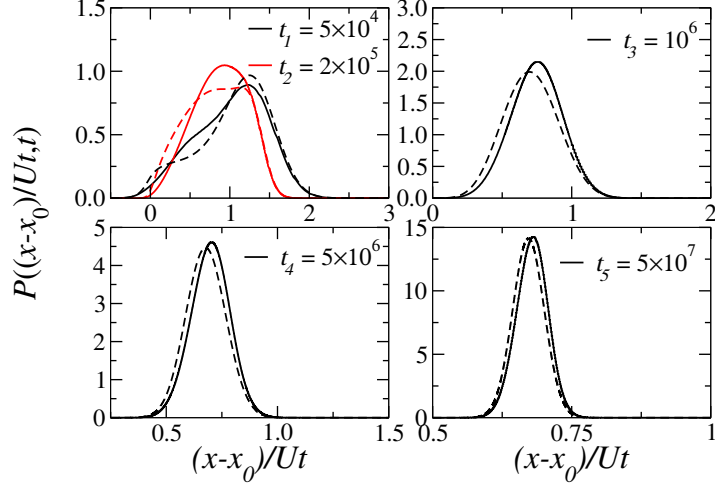


Figure 4: Normalized propagator  $P((x - x_0)/Ut, t)$  observed at different times  $t_n$ . The solid and dashed lines denote the results for Henry and Langmuir adsorption, respectively. These results were obtained with  $k_H = k_L = 10$ ,  $Pe = 25$ ,  $\Gamma^\infty = 1$  and  $c_0 = 10$ . color online only

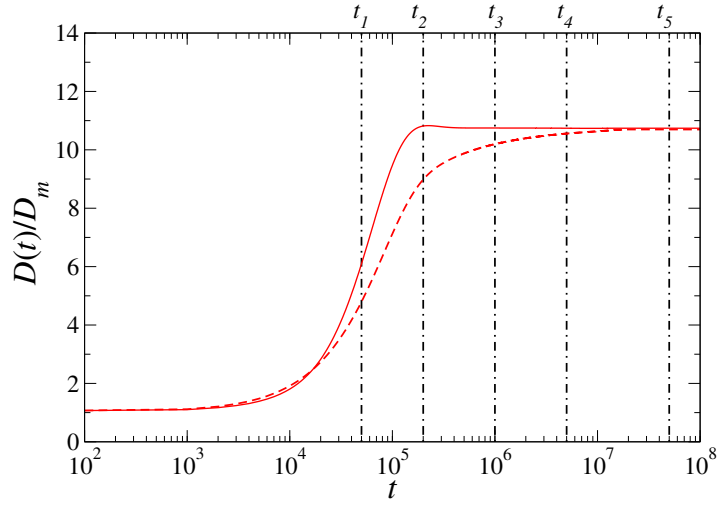


Figure 5: Dispersion coefficient  $D(t)$ , which is normalized by the molecular diffusion coefficient  $D_m$  of the free, i.e. non-adsorbing, tracers. The solid and dashed red lines correspond to molecules adsorbing to the pore surface according to Henry and Langmuir adsorption, respectively. The adsorption/desorption rates are  $k_H = k_L = 10$  and  $\Gamma^\infty = 1$ . The vertical dotted lines denote different times  $t_n$ . The system parameters are  $Pe = 25$  and  $c_0 = 10$ . color online only

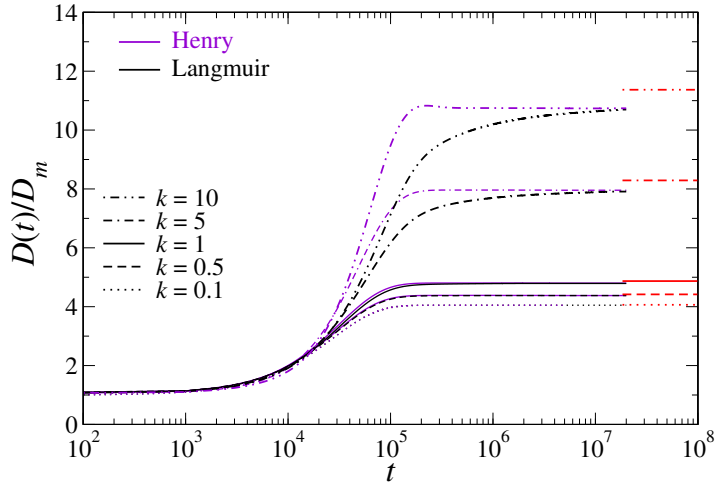


Figure 6: Dispersion coefficient  $D(t)$ , which is normalized by the molecular diffusion coefficient  $D_m$  of the free, i.e. non-adsorbing, tracer molecules. The system parameters are  $\Gamma^\infty = 1$   $Pe = 25$  and  $c_0 = 10$ . The purple and black colors denote data for the Henry and Langmuir adsorption isotherms while the red horizontal lines denote the analytical values for  $D_{eff}^{ads}/D_m$ . The lines (dotted, dashed, solid, dashed-dotted, double-dashed-dotted and dashed-double-dotted) denote different values of  $k = k_L = k_H$  (0.1, 0.5, 1, 5 and 10, respectively). color online only

so-called Taylor dispersion regime. Moreover,  $D_{eff}^{ads}/D_m$  increases with  $k$  as the resulting displacement difference between adsorbed and non-adsorbed molecules leads to a larger variance.  $D_{eff}^{ads}/D_m$  for both models, which are very close to each other, match very well the known analytical solution for Henry adsorption. However, the duration of the intermediate advection-dominated regime for the Langmuir model increases for higher values of  $k$ . This difference is due to the fact that the desorbed amount of molecules following the Langmuir adsorption isotherm is not directly proportional to the variation in the concentration near the surface (as it is the case for the Henry adsorption isotherm). Such an effect is particularly important in the plateau region of the adsorption isotherm. Moreover, while the difference observed between the two adsorption models is very small for small  $k$ , it becomes more pronounced upon increasing  $k$  to large values.

### 3.3. Large adsorption/desorption ratios

As can be seen from Fig. 6,  $D(t)/D_m$  for the molecules obeying Henry adsorption shows a slight overshoot at the end of the advection regime for

$k_H = 10$ . Considering that this effect is not observed for the Langmuir model, we expect it to be related to the absence of adsorption-induced surface saturation. To gain insights into this phenomenon, we performed simulations using Henry's law with a constant initial concentration  $c_0 = 10$  with various adsorption/desorption ratios  $k_H$  (by modifying the adsorption rate parameter  $p_A$  for constant  $p_D$ ). More in detail, a constant desorption rate  $p_D = 0.001$  is used while performing simulations with  $k_H = 10, 40, 100$  (e.g.  $p_A = 0.01, 0.04, 0.1$ , respectively). Fig. 7 shows the normalized time derivative of the displacement variance  $D(t)/D_m$  as a function of time  $t$ . Upon increasing  $k_H$ ,  $D(t)/D_m$  displays a peak (maximum) before reaching the dispersive regime. However, regardless of the value of  $k_H$ , the three main transport regimes are still observed: diffusion, advection, and dispersion. The maximum observed in the time evolution of  $D(t)/D_m$  is specific to the use of adsorbing conditions without surface saturation (allowing the adsorption of a very large quantity directly after injection on a time scale that is much shorter than a characteristic time of the transporting fluid). Moreover, as the adsorption rate is much higher than the desorption rate, desorption is a slower process. To better illustrate this effect, Fig. 8 shows the free and adsorbed tracer concentration fields for different  $k_H$ . The data obtained at  $t = t_2$  indicate that the free molecules are distributed according to the Poiseuille velocity profile whereas a specific amount of molecules is adsorbed to the surface close to the inlet  $x_0$ . As expected, the adsorbed amount increases with  $k_H$ . For larger  $t$  ( $t = t_4, t = t_5$ ) and  $k_H = 40$  and  $k_H = 100$ , one observes two regions characterized by higher concentrations. These specific regions correspond to (1) molecules in the center of the channel carried by the velocity field and (2) molecules having been adsorbed to the surface and then released due to the desorption process. We note that this effect becomes more pronounced if  $k_H$  increases as the impact of adsorption becomes more important. The existence of these two spatially separated populations explains the overshoot observed in  $D(t)/D_m$ . At larger times,  $t = t_6, t = t_7$  and  $t = t_8$ , the contrast between the two populations fades out and the concentration in free molecules becomes more homogeneously distributed within the geometry. In this asymptotic (long-time) limit,  $D(t)/D_m$  decreases and eventually reaches the plateau value that characterizes the dispersive regime.

Fig. 9 shows the normalized propagators  $P[(x - x_0)/Ut, t]$  for the different systems at specific times  $t_n$ . For  $t = t_2$ , the system is at the onset of the advective regime where the tracer concentration has been displaced by a small amount only. Therefore, in this short time interval, the influence of the

1  
2  
3  
4  
5  
6  
7  
8  
9  
10  
11  
12  
13  
14  
15  
16  
17  
18  
19  
20  
21  
22  
23  
24  
25  
26  
27  
28  
29  
30  
31  
32  
33  
34  
35  
36  
37  
38  
39  
40  
41  
42  
43  
44  
45  
46  
47  
48  
49  
50  
51  
52  
53  
54  
55  
56  
57  
58  
59  
60  
61  
62  
63  
64  
65

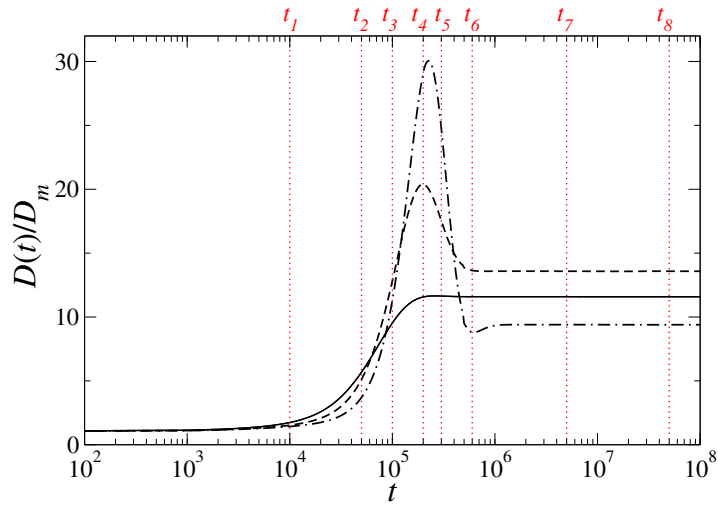


Figure 7: Dispersion coefficient  $D(t)$ , which is normalized by the molecular diffusion coefficient  $D_m$  of the free, i.e. non-adsorbing, tracer molecules. Molecules adsorb according to a Henry adsorption model with different adsorption/desorption rates  $k_H$ . The solid, dashed and dotted-dashed lines denote  $k_H = 10$ , 40 and 100, respectively. The vertical dotted lines denote different times  $t_n$ . The system is characterized by  $Pe = 25$  and an initial concentration  $c_0 = 10$ . color online only

adsorption ratio  $k_H$  is not pronounced as most of the molecules are still located near the injection position  $x_0$ . In the advection dominated regime, i.e. for  $t = t_3, t_4$  and  $t_5$ , the three data sets exhibit more pronounced differences when varying  $k_H$ . The propagators display a plateau for small normalized displacements and a peak for large  $(x - x_0)/Ut$ . However, for  $k_H = 40$  and  $k_H = 100$ , the propagators show an additional peak close to  $(x - x_0)/Ut = 0$ . These peaks at large and small normalized displacements correspond to two different subpopulations: (1) non-adsorbed molecules transported by the velocity field and (2) molecules adsorbed directly after injection and released later on. For  $t = t_4$ , the propagators obtained with  $k_H = 10$  are of a quasi-Gaussian shape, which suggests that the end of the advection-dominated regime is reached. However, for  $k_H = 40$  and  $k_H = 100$ , where  $D(t)/D_m$  is maximum at  $t = t_4$ , the adsorption effect on the normalized propagators is still very pronounced. For these cases, the advection-dominated regime ends at a larger time. For  $t = t_6$ , the data for  $k_H = 10$  correspond to a propagator that has a nearly Gaussian shape. In contrast, owing to more significant adsorption effects, the data for  $k_H = 40$  and  $100$  correspond to an asymmetric propagator which has not yet reached a Gaussian shape. For  $t = t_7$ , all propagators become closer to ideal Gaussian distributions but the differences observed between the data sets reflect the effect of the adsorption/desorption ratio  $k_H$ . Propagators are shifted to the left with respect to non-adsorbing conditions with a shift that increases upon increasing the adsorption/desorption ratio. These results further indicate that adsorption drastically delays tracer dispersion in porous media.

#### 3.4. Influence of initial concentration $c_0$

In this section, we assess the influence of the initial concentration  $c_0$  on the dispersion of molecules adsorbing according to the Langmuir adsorption model. As can be inferred from the known analytical solution,  $D(t)/D_m$  of molecules adsorbing according to Henry's law is independent of  $c_0$  (due to the fact that this simple model does not account for surface saturation). In contrast, with the Langmuir adsorption model, we expect an important impact of the initial concentration on tracer dispersion in adsorbing conditions. In a first step, we investigate the time evolution of  $D(t)/D_m$  for  $c_0 = 10, 20, 30$ . Then, we vary  $c_0$  from 10 to 1000 to study the influence of higher initial concentrations on  $D(t)/D_m$  but also on the concentration fields and associated propagators. Fig. 10 presents  $D(t)/D_m$  for molecules adsorbing according to Henry and Langmuir adsorption isotherms with different

1  
2  
3  
4  
5  
6  
7  
8  
9  
10  
11  
12  
13  
14  
15  
16  
17  
18  
19  
20  
21  
22  
23  
24  
25  
26  
27  
28  
29  
30  
31  
32  
33  
34  
35  
36  
37  
38  
39  
40  
41  
42  
43  
44  
45  
46  
47  
48  
49  
50  
51  
52  
53  
54  
55  
56  
57  
58  
59  
60  
61  
62  
63  
64  
65

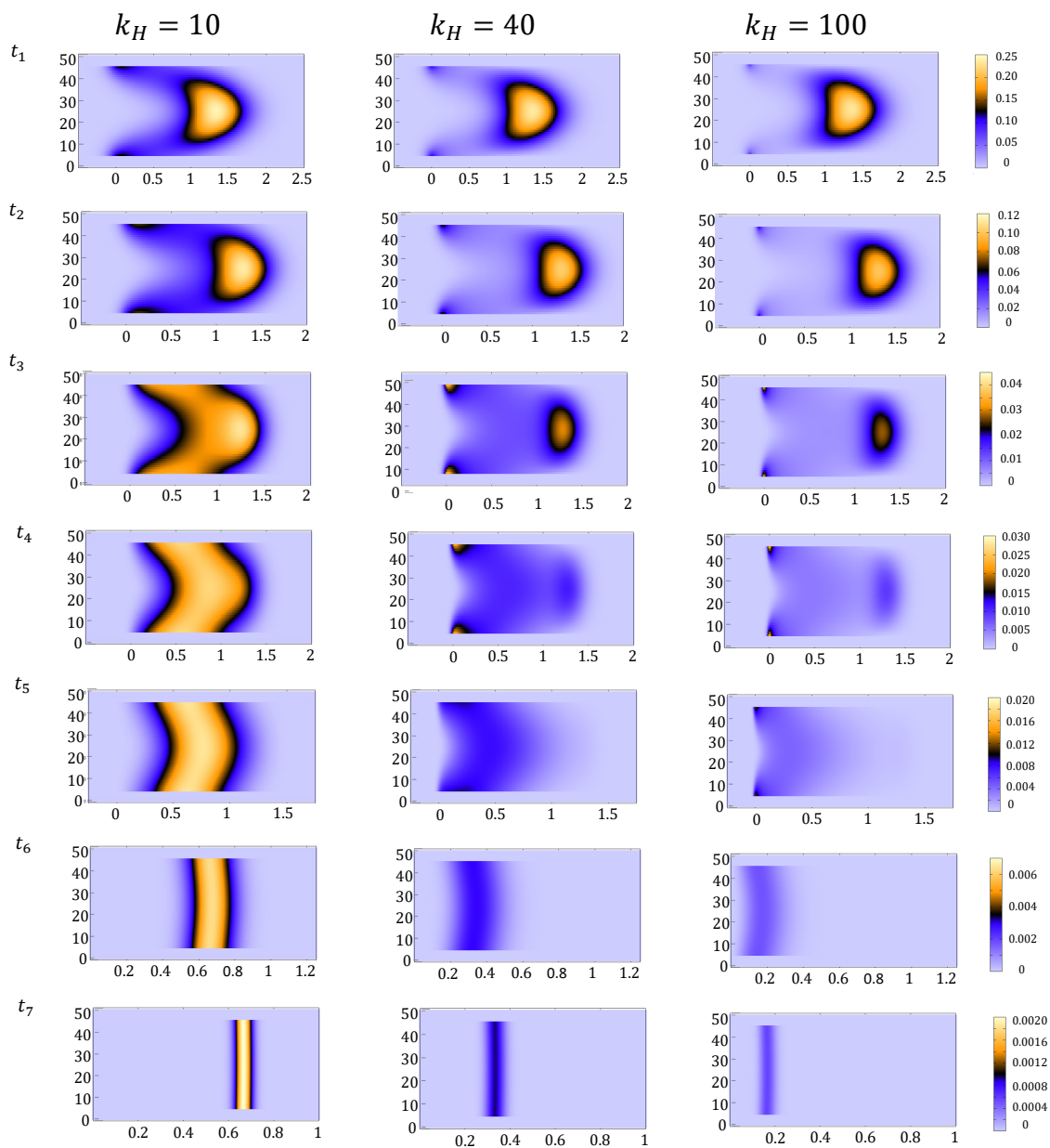


Figure 8: Concentration fields observed at different times  $t_n$  for molecules adsorbing according to a Henry adsorption isotherm with different  $k_H$ . The different panels present the concentration fields for  $k_H = 10$ ,  $k_H = 40$  and  $k_H = 100$ , respectively. The abscissas are plotted in units of  $(x - x_0)/Ut$  where  $x_0$  is the lateral injection position and  $U$  is the mean flow velocity. The Peclet number is  $Pe = 25$  and the initial concentration  $c_0 = 10$ .

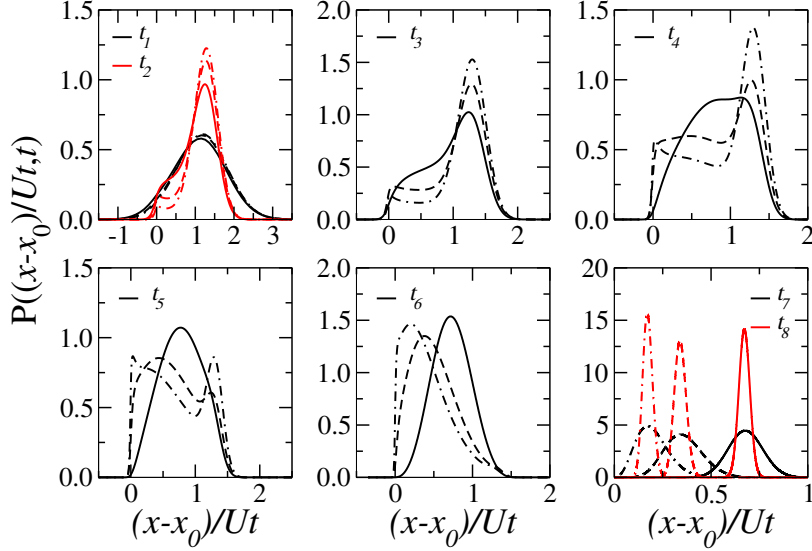


Figure 9: Normalized propagators  $P((x - x_0)/Ut, t)$  observed at different times  $t_n$  – as shown in Fig. 6. The solid, dashed and dotted-dashed lines denote the data for  $k_H = 10$ , 40 and 100, respectively. color online only

adsorption/desorption rates  $k = k_L = k_H$ . Different initial concentrations  $c_0 = 10, 20, 30$  were considered for the calculations with the Langmuir adsorption isotherm. As can be seen, the dispersion of tracer molecules following the Langmuir adsorption model shows a marked  $c_0$ -dependency. Such dependency becomes more pronounced for larger  $c_0$  and  $k$ . Moreover, for large  $k$ , the difference between the Langmuir and Henry models becomes more important. To disentangle the influence of the initial concentration  $c_0$  from the effect of  $k$ , we normalize  $D(t)$  with respect to its value in the infinite time limit  $D(t \rightarrow \infty)$ . We present  $D(t)$  in the Supplemental Information as obtained with  $k = 0.5$  and  $k = 1$ . These results indicate that the difference between the Henry model and the different Langmuir adsorption models is more pronounced for  $k = 1$  than for  $k = 0.5$  – therefore, suggesting that the effect of the initial concentration  $c_0$  on the Langmuir adsorption is more pronounced when using a higher adsorption/desorption ratio  $k$ . Finally, it can be seen from Fig. 10 that  $D(t)/D_m$  for  $k = 10$  and  $c_0 = 10; 20; 30$  does not reach the Taylor dispersion plateau in the investigated time range.

Fig. 11 shows the time evolution of the free tracer concentration field along the normalized x-axis  $(x - x_0)/Ut$  for molecules adsorbing according to the

1  
2  
3  
4  
5  
6  
7  
8  
9  
10  
11  
12  
13  
14  
15  
16  
17  
18  
19  
20  
21  
22  
23  
24  
25  
26  
27  
28  
29  
30  
31  
32  
33  
34  
35  
36  
37  
38  
39  
40  
41  
42  
43  
44  
45  
46  
47  
48  
49  
50  
51  
52  
53  
54  
55  
56  
57  
58  
59  
60  
61  
62  
63  
64  
65

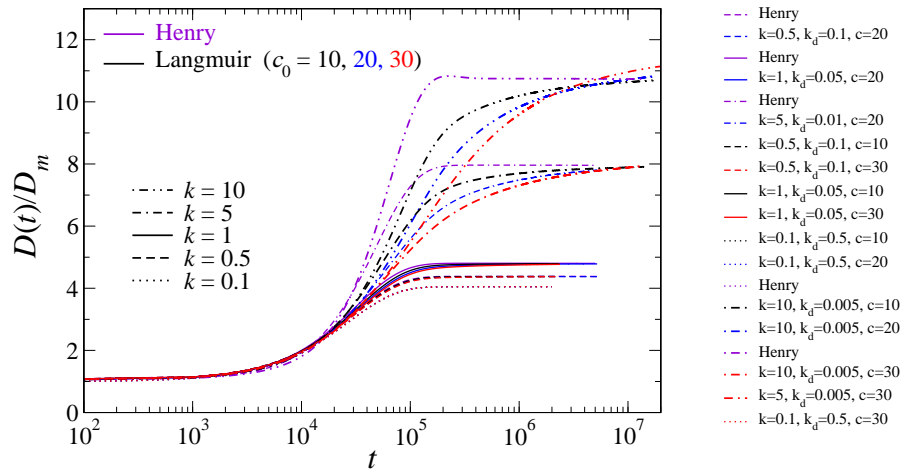


Figure 10: Dispersion coefficient  $D(t)$ , which is normalized to the molecular diffusion coefficient  $D_m$  of free tracer molecules. In these calculations, the molecules adsorb according to the Henry or Langmuir adsorption model. The black, blue and red colors denote data obtained with the Langmuir adsorption isotherm for different initial concentrations ( $c_0 = 10$ ,  $c_0 = 20$ ,  $c_0 = 30$ ). The violet color denotes the data obtained with the Henry adsorption isotherm for  $c_0 = 10$ . The lines (dotted, dashed, solid, dashed-dotted, double-dashed-dotted and dashed-double-dotted) denote data obtained for different  $k = k_L = k_H$  (0.1, 0.5, 1, 5 and 10, respectively). These data were obtained for  $\Gamma^\infty = 1$  and  $Pe = 25$ .  
color online only

1  
 2  
 3  
 4  
 5  
 6 Langmuir adsorption model. We also show the corresponding normalized  
 7 propagators for the following initial concentrations:  $c_0 \in \{10, 30, 500\}$  with  
 8  $k_L = 10$  and  $\infty = 1$  in Fig. 12. Fig. 11 shows that the concentration field for  
 9  $c_0 = 10$  at  $t = t_1$  is strongly affected by adsorption as the two subpopulations  
 10 – corresponding to transported non-adsorbed molecules and to adsorbed-  
 11 then-released molecules – can be observed. As can be seen from these data, a  
 12 non-negligible part of the molecules are delayed due to adsorption. However,  
 13 for  $c_0 = 500$ , at  $t = t_1$ , the concentration field is barely affected by the  
 14 velocity field which obeys a Poiseuille flow profile. Due to surface saturation,  
 15 only a certain amount of molecules independent of the initial concentration  
 16 is adsorbed at the surface. For  $t = t_2$ , the spreading of the concentration  
 17 around the mean position becomes more symmetrical – particularly for  $c_0 =$   
 18  $10$  and  $c_0 = 30$  as can be seen from the propagators in Fig. 12. For  
 19  $t = t_4$  and  $t = t_5$ , in the case of low initial concentrations, the dispersion  
 20 regime is reached as the propagators display a Gaussian shape. Moreover,  
 21 the propagators are shifted towards smaller normalized displacements due  
 22 to adsorption. However, for  $t = t_3$ , when large initial concentrations  $c_0$  are  
 23 considered, the onset of tailing of the concentration fields and propagators  
 24 for smaller  $(x - x_0)/Ut$  can be observed. Tailing, which corresponds to  
 25 spreading of molecules far behind the tracer front, is due to the desorption  
 26 of the initially adsorbed molecules. However, at this instant, the propagator  
 27 center is located at  $(x - x_0)/Ut = 1$  with a nearly Gaussian shape (resulting  
 28 from the fact that most molecules were not yet adsorbed due to adsorption  
 29 limitations induced by surface saturation). In contrast, for larger  $t$ , tailing  
 30 becomes more pronounced and the propagator shape is clearly not Gaussian.

31  
 32 To gain further insight into the influence of large  $c_0$  on transport of adsorb-  
 33 ing molecules, we present in Fig. 13 the time evolution of  $D(t)/D_m$  for a large  
 34 range of initial concentrations. For low concentrations, i.e.  $c_0 \in [10, 100]$ , the  
 35 typical transport regimes are observed. Upon increasing the initial concen-  
 36 tration, i.e. for  $c_0 = 75$  and  $c_0 = 100$ , the advective regime extends over a  
 37 longer time so that the time required to reach the dispersive regime becomes  
 38 longer. This effect is due to the shape of the Langmuir adsorption isotherm  
 39 which involves larger concentration variations leading to adsorption equilib-  
 40 rium. For systems with larger initial concentrations, i.e. for  $c_0 > 200$ , the  
 41 time evolution of  $D(t)/D_m$  is different than at lower initial concentrations.  
 42 We notice that the advective regime is divided into two stages which are sep-  
 43 arated by a short stationary regime (small plateau). The latter regime, which  
 44 corresponds to the onset of the Taylor dispersion regime, can be explained

1  
2  
3  
4  
5  
6  
7  
8  
9  
10  
11  
12  
13  
14  
15  
16  
17  
18  
19  
20  
21  
22  
23  
24  
25  
26  
27  
28  
29  
30  
31  
32  
33  
34  
35  
36  
37  
38  
39  
40  
41  
42  
43  
44  
45  
46  
47  
48  
49  
50  
51  
52  
53  
54  
55  
56  
57  
58  
59  
60  
61  
62  
63  
64  
65

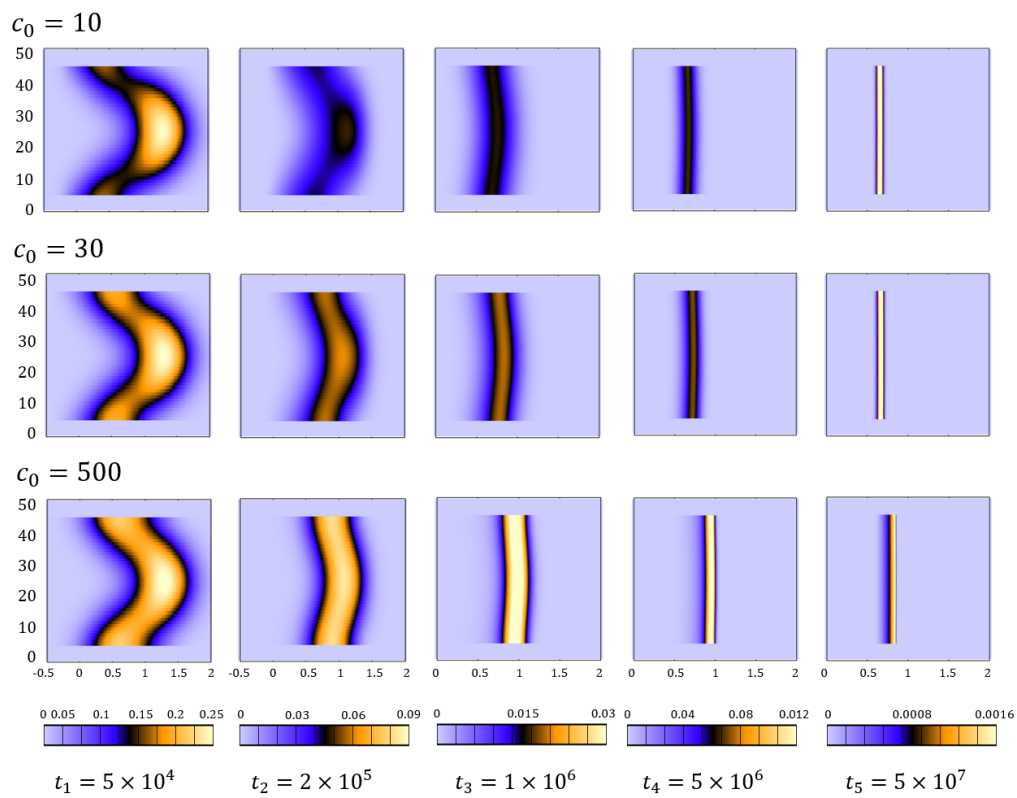


Figure 11: Concentration fields observed at different times  $t_n$  for transported tracer molecules adsorbing according to a Langmuir adsorption isotherm. The top, middle and bottom data are for  $c_0 = 10, 30$  and  $500$ , respectively. Concentration scales are normalized by  $c_0/10$ . The abscissas are plotted in units of  $(x - x_0)/Ut$ . The results correspond to the dispersion of molecules obeying a Langmuir adsorption isotherm with  $k_L = 10$  and  $\Gamma^\infty = 1$ . The systems considered here are characterized by Peclet number  $Pe = 25$ .

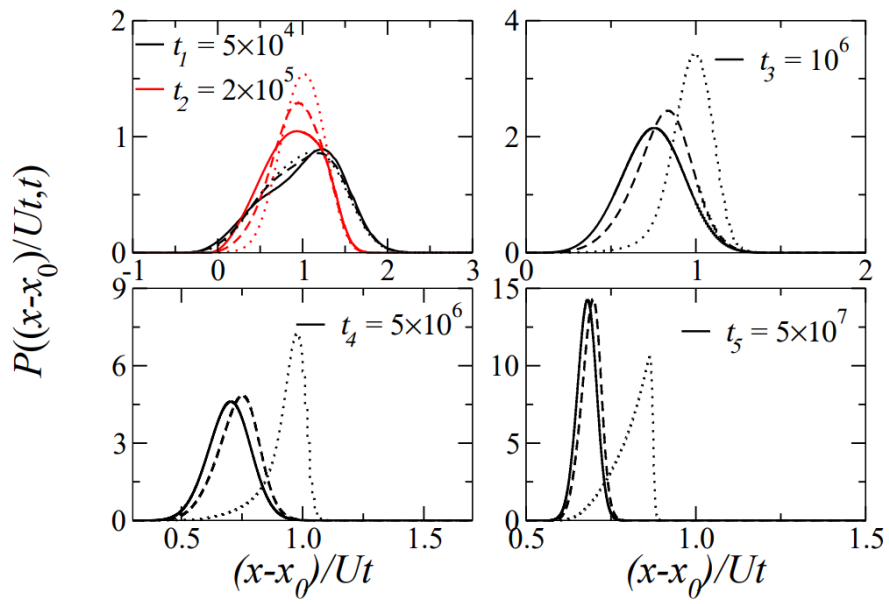


Figure 12: Normalized propagator  $P((x - x_0)/Ut, t)$  observed at different times  $t_n$ . The solid, dashed and dotted lines correspond to data obtained for the Langmuir adsorption model with an initial concentrations  $c_0 = 10, 30$  and  $500$ , respectively. The same configuration and adsorbing conditions as in Fig. 11 are used. color online only

1  
2  
3  
4  
5  
6  
7  
8  
9  
10  
11  
12  
13  
14  
15  
16  
17  
18  
19  
20  
21  
22  
23  
24  
25  
26  
27  
28  
29  
30  
31  
32  
33  
34  
35  
36  
37  
38  
39  
40  
41  
42  
43  
44  
45  
46  
47  
48  
49  
50  
51  
52  
53  
54  
55  
56  
57  
58  
59  
60  
61  
62  
63  
64  
65

by the fact that the concentration of free, not yet adsorbed, tracers in the bulk is very high. With  $\Gamma^\infty = 1$ , the impact of the adsorbed molecules on the displacement variance of the free molecules is negligible at the beginning of the transport process. At larger times, the free tracers get dispersed in the channel so that their concentration becomes comparable to the concentration of molecules that were already adsorbed. As a result, the effect of adsorption on transport becomes more important and  $D(t)/D_m$  increases until reaching the asymptotic dispersion regime at very long times.

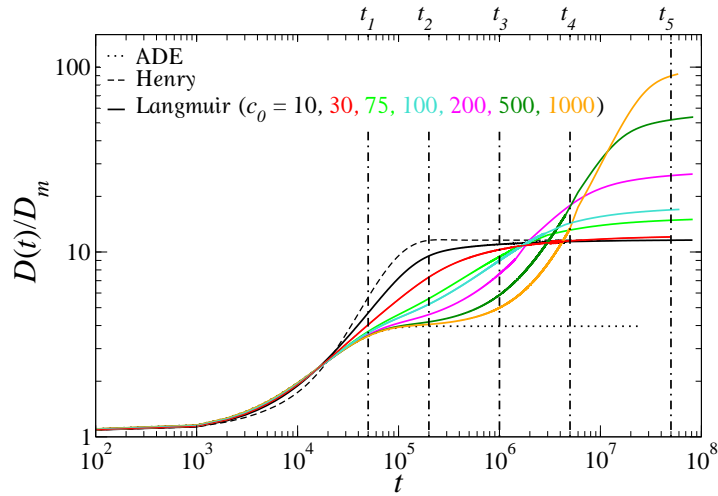


Figure 13: Dispersion coefficient  $D(t)$ , which is normalized by the molecular diffusion coefficient  $D_m$  of the free tracer molecules. We consider the dispersion of molecules that obey different adsorption models with  $k = 10$ . The dotted, dashed and solid lines correspond to the dispersion of non-adsorbing molecules, molecules following the Henry model and molecules following the Langmuir model, respectively. The black color corresponds to data for systems with an initial concentration  $c_0 = 10$ . The systems considered here are characterized by  $Pe = 25$ . color online only

### 3.5. Cooperative model upon continuous injection

In this section, we compare the transport of molecules adsorbing according to the Henry and Langmuir models with that observed for molecules adsorbing according to the cooperative model. To do so, we consider an advanced thermodynamic model that was developed recently to describe adsorption of self-aggregating molecules such as surfactants on silica (Zaafouri et al. (2020)). As described above, this cooperative adsorption model allows

1  
 2  
 3  
 4  
 5  
 6  
 7  
 8  
 9 describing the adsorption of individual and aggregated monomers. On the  
 10 one hand, the adsorption of individual monomers follows Henry's law with  
 11 an adsorption/desorption ratio  $k_H$ . Maximal surface saturation of individual  
 12 monomers is reached at the critical micellar concentration CMC. Above the  
 13 CMC, the adsorbed quantity of individual monomers remains constant. If the  
 14 concentration is higher than the so-called critical surface concentration  $c_s$  (in  
 15 the present case we have  $c_s < CMC$ ), aggregated monomers adsorb at the  
 16 surface following a surface concentration-dependent adsorption/desorption  
 17 ratio  $k'(\Gamma_{m'})$ . To avoid the drastic concentration decrease observed upon a  
 18 Dirac pulse injection, we use here a continuous injection over a certain time  
 19 as described before. Data for Dirac pulse injection in combination with the  
 20 Henry and cooperative adsorption models are given in the Supplemental In-  
 21 formation file. In practice, the Peclet number is  $Pe = 100$  and an initial  
 22 concentration  $c_0 = 1000$  is injected at a lateral position  $x_0 = 1$  over a time  
 23 period  $\Delta t_0 = 10^5 \Delta t$ . The parameters for the Henry, Langmuir and coopera-  
 24 tive models are given in Fig. 2 and Fig. S1 (Supplemental Information file).  
 25 Fig. 14 shows the adsorbed amount  $\Gamma(x)$  as a function of the lateral position  
 26 for the Henry, Langmuir and cooperative models at different times as well as  
 27 the surface and bulk concentrations.  $\Gamma(x)$  for the Langmuir model already  
 28 increases for very low surface concentrations. Due to the spreading of the  
 29 concentration over time, the total adsorbed amount ( $\int_x \Gamma(x, t) dx$ ) becomes  
 30 very important. In contrast to this model,  $\Gamma(x)$  for the cooperative model  
 31 follows  $\Gamma(x)$  observed for the Henry model in the low concentration regime.  
 32 For  $c_{surf} > c_s$ , a strong increase in  $\Gamma(x)$  can be observed due to the coop-  
 33 erative effect at play upon aggregated monomer adsorption. Then, for even  
 34 larger  $c_{surf}$ , the curve flattens following the plateau region of the adsorp-  
 35 tion isotherm. The total amount of adsorbed molecules is lower than for the  
 36 Langmuir model. Fig. 15 shows  $\int_x \Gamma(x, t) dx$  for both models. As can be seen,  
 37  $\int_x \Gamma(x, t) dx$  for the Langmuir model increases rapidly and does not reach a  
 38 constant limit (Fig. 15). Fig. 16 shows the the difference in bulk concen-  
 39 tration between the two models ( $c_{bulk,LC} - c_{bulk,L}$ ) at different times. Whereas  
 40 the bulk concentration of the cooperative model particularly decreases in  
 41 the center of the concentration profile, bulk concentration of the Langmuir  
 42 model decreases in the front and the tail of the concentration profile due to  
 43 the adsorption at lower concentrations.  
 44  
 45  
 46  
 47  
 48  
 49  
 50  
 51  
 52  
 53  
 54  
 55  
 56  
 57  
 58  
 59  
 60  
 61  
 62  
 63  
 64  
 65

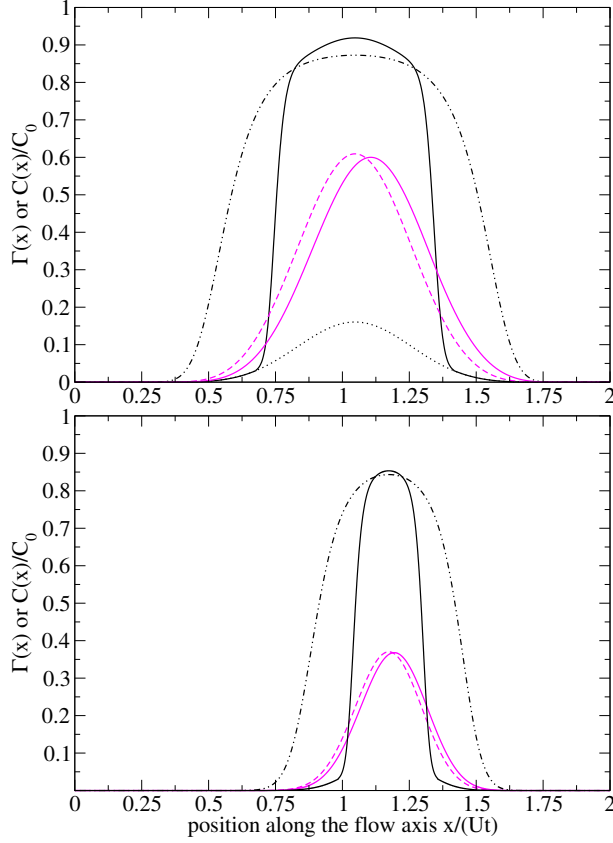


Figure 14: Adsorbed amount  $\Gamma(x)$  and normalized bulk concentration  $c(x)/c_0$  along the flow axis at a time step  $t = 4 \times 10^5 t_{LB}$  (top) and  $t = 1.1 \times 10^6 t_{LB}$  (bottom). The Peclet number is  $Pe = 100$ . For both figures, the dotted, dashed-dotted and solid black lines are the adsorbed amount  $\Gamma(x)$  for the Henry, Langmuir and cooperative adsorption models, respectively. The pink dashed line corresponds to the surface concentration distribution while the pink solid line represents the bulk distribution. color online only

#### 4. Conclusion

We investigated the interplay between surfactant adsorption kinetics and transport using a Lattice Boltzmann method within the Two Relaxation Time approach. This method ensures that accurate results are obtained for molecule transport in simple and complex pore geometries. We focused on two principal subjects: First, the different transport regimes, and particularly the transient regimes, whose understanding is crucial for the description and prediction of transport of adsorbing molecules in porous media. To

1  
2  
3  
4  
5  
6  
7  
8  
9  
10  
11  
12  
13  
14  
15  
16  
17  
18  
19  
20  
21  
22  
23  
24  
25  
26  
27  
28  
29  
30  
31  
32  
33  
34  
35  
36  
37  
38  
39  
40  
41  
42  
43  
44  
45  
46  
47  
48  
49  
50  
51  
52  
53  
54  
55  
56  
57  
58  
59  
60  
61  
62  
63  
64  
65

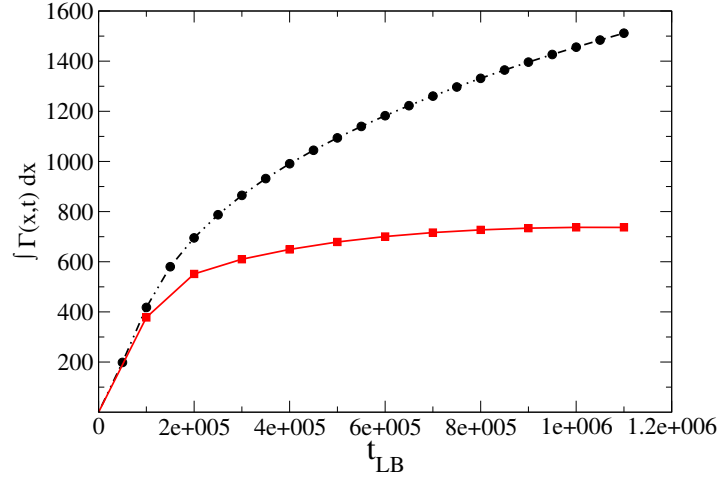


Figure 15: Total adsorbed amount as a function of time  $t$  for the Langmuir adsorption model (circles) and the cooperative adsorption model ( $\beta = 0.5$ , squares). In both cases, the Peclet number is  $Pe = 100$ . color online only

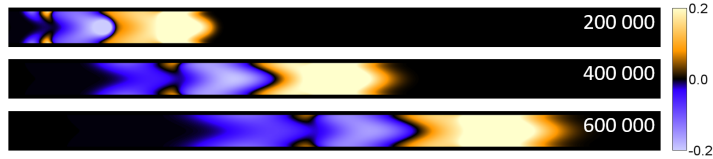


Figure 16: Difference in bulk concentration between the cooperative adsorption model and the Langmuir model ( $c_{bulk,LC} - c_{bulk,L}$ ) at three different times. For the sake of clarity, these data focus on the first third of the channel and the original aspect ratio is not respected ( $51 \times 3500$  pixels). color online only

this goal, we studied the influence of system parameters such as the initial concentration  $c_0$  and the adsorption/desorption ratio  $k$  on the temporal coupling between transport and adsorption. Second, we presented transport of complex molecules, as for example micropollutants and surfactants, whose adsorption behavior is dominated by cooperative effects.

#### Transient regimes and their dependence on system parameters

In the pore geometry, the dispersion of adsorbing molecules that obey the Henry adsorption model follows the same qualitative evolution for  $D(t)/D_m$  as that for non-adsorbing molecules. More in detail, the three following regimes are observed: diffusion, advection-dominated transport, and dispersion. Interestingly, the transport of adsorbing molecules leads to a disper-

sive regime with an effective dispersion coefficient that is larger than that for non-adsorbing molecules. This is due to adsorption conditions at the surface of the parallel plate geometry which leads to an increase in the displacement variance  $\sigma_x^2(t)$  in the  $x$ -direction (flow direction). Moreover, the adsorption/desorption ratio  $k_H$  is found to significantly affect the observed transport regimes since large  $k_H$  yield strong adsorption effects near the lateral injection position (due to the linearity between the concentration and the adsorbed quantity in the Henry model). The corresponding large adsorbed amount remains trapped at the surface over long residence times. In practice, this leads to the appearance of an additional step during the advection-dominated regime: the increase in the displacement variance  $D(t)/D_m$  reaches a maximum before decreasing to its asymptotic value as adsorbed and free molecules get redistributed/exchanged.

To study the influence of surface saturation, we modeled in a second part the transport of molecules obeying the Langmuir adsorption model. The results show that the initial concentration  $c_0$  has an important effect on the transport regimes. Moreover, we also found that this dependence on initial concentration is more pronounced as the adsorption/desorption ratio  $k$  increases. This effect arises during the advection-dominated regime, which extends over longer times with a significant increase in the effective dispersion coefficient. Using large initial concentrations ( $c_0 > 200$ ), the advection regime consists of two stages which are connected by a stationary regime. During the first stage, the free molecule distribution is not affected by adsorption as an intermediate stationary regime is reached for  $D(t)/D_m$ ; this regime corresponds to the Taylor dispersion regime. Then, during the second stage,  $D(t)/D_m$  increases until it reaches the dispersion regime with a value characteristic of the transport of the molecules adsorbing according to the Langmuir adsorption model. This effect is due to the strong contrast between the free and adsorbed tracer concentrations.

**Cooperative adsorption** Finally, considering Dirac pulse injection with a cooperative adsorption model, we studied the influence of such a collective behavior at concentrations larger than the critical surface concentration  $c_s$ . However, even for a large initial concentration  $c_0$ , owing to such cooperative adsorption, the bulk concentration decreases quickly after injection so that the surface concentration is always in the Henry regime (where only monomer adsorption occurs). To extend our study to more relevant regimes, we therefore performed simulations with continuous concentration injection. By monitoring the evolution of the adsorbed amounts corresponding to iso-

1  
2  
3  
4  
5  
6  
7  
8  
9  
10  
11  
12  
13  
14  
15  
16  
17  
18  
19  
20  
21  
22  
23  
24  
25  
26  
27  
28  
29  
30  
31  
32  
33  
34  
35  
36  
37  
38  
39  
40  
41  
42  
43  
44  
45  
46  
47  
48  
49  
50  
51  
52  
53  
54  
55  
56  
57  
58  
59  
60  
61  
62  
63  
64  
65

lated and aggregated monomers ( $\Gamma_m(x, t)$  and  $\Gamma_{m'}(x, t)$ ), we checked the accuracy/validity of the kinetics implementation for the cooperative adsorption model in the LBM-TRT algorithm. Important differences between the adsorption models could be observed in the temporal evolution of the concentration profiles and the total adsorbed amount. Indeed, the total amount of adsorbed molecules estimated by the Langmuir model is much larger than the one of the cooperative model as it does not account for separated monomer and aggregate adsorption. In this case, spreading of the tracer distribution due to dispersion leads to very large adsorbed amounts.

In conclusion, our findings illustrate the stringent need to include specific adsorption modeling, including system parameters coherent with experimental data, into transport models to obtain a physically consistent adsorption/transport behavior. Indeed, we have shown, that system parameters as well as the type of adsorption model strongly influence the transient transport regimes and hence the temporal and spatial concentration distribution. Such understanding provides crucial help to rationalize transport behavior of molecules subject to adsorption in porous media. Consequently, in the context of water remediation simulations in the presence of surfactants and/or micro-pollutants (microplastics, metals, pharmaceutical molecules and PPCP), it is crucial to include a robust thermodynamic adsorption model, specific for each molecule, which allows taking into account the rich and complex physicochemical behavior of these molecules.

In future works, a challenging task will consist of investigating the coupling between transport and adsorption in more complex porous structures. Indeed, the heterogeneity of the porous medium induces a specific velocity field with high and low velocity zones and, hence, a more complex dispersion behavior that influences adsorption. In practice, this implies that different characteristic times in the velocity field compete with relevant adsorption rates. The knowledge of the macroscopic transport equations therefore becomes crucial in the context of the description of pollutant transport in porous media.

Agarwal, S., Verma, N., Mewes, D., 2005. A lattice boltzmann model for adsorption breakthrough. *Heat and Mass Transfer* 41 (9), 843–854.

Appadu, A., 2016. Comparative study of three numerical schemes for contaminant transport with kinetic langmuir sorption. In: *AIP Conference Proceedings*. Vol. 1738. AIP Publishing LLC, p. 030021.

- 1  
2  
3  
4  
5  
6  
7  
8  
9 Asta, A., Levesque, M., Rotenberg, B., 2018. Moment propagation method  
10 for the dynamics of charged adsorbing/desorbing species at solid-liquid  
11 interfaces. *Molecular Physics* 116, 2965–2976.  
12  
13 Batôt, G., Talon, L., Peysson, Y., Fleury, M., Bauer, D., 2016. Analytical  
14 and numerical investigation of the advective and dispersive transport in  
15 herschel–bulkley fluids by means of a lattice–boltzmann two-relaxation-  
16 time scheme. *Chemical Engineering Science* 141, 271–281.  
17  
18 Bear, J., 2018. Modeling transport of chemical species. In: *Modeling Trans-*  
19 *port of Chemical Species*. Springer.  
20  
21 Bear, J., Cheng, A., 2010. Modeling groundwater flow and contaminant  
22 transport. In: *Modeling Groundwater Flow and Contaminant Transport*.  
23 Springer.  
24  
25 Berezkhovskii, A. M., Skvortsov, A. T., 2013. Aris-taylor dispersion with  
26 drift and diffusion of particles on the tube wall. *The Journal of Chemical*  
27 *Physics* 139 (8), 084101.  
28  
29 Boek, E., Zacharoudiou, I., Gray, F., Shah, S., Crawshaw, J., Yang, J., 2017.  
30 Multiphase-flow and reactive-transport validation studies at the pore scale  
31 by use of lattice boltzmann computer simulations. *SPE Journal* 22 (940).  
32  
33 Boțan, A., Ulm, F.-J., Pellenq, R. J.-M., Coasne, B., 2015. Bottom-up model  
34 of adsorption and transport in multiscale porous media. *Physical Review*  
35 *E* 91, 032133.  
36  
37 Coasne, B., 2016. Multiscale adsorption and transport in hierarchical porous  
38 materials. *New Journal of Chemistry* 40, 4078.  
39  
40 Coasne, B., Galarneau, Anne and Gerardin, C., Fajula, F., Villemot, F., 2013.  
41 Molecular simulation of adsorption and transport in hierarchical porous  
42 materials. *Langmuir* 29 (25), 7864–7875.  
43  
44 Denoyel, R., Rouquerol, J., 1991. Thermodynamic (including microcalorime-  
45 try) study of the adsorption of nonionic and anionic surfactants onto silica,  
46 kaolin, and alumina. *Journal of Colloid and Interface Science* 143 (2), 555–  
47 572.  
48  
49  
50  
51  
52  
53  
54  
55  
56  
57  
58  
59  
60  
61  
62  
63  
64  
65

- 1  
2  
3  
4  
5  
6  
7  
8  
9 Eerkes-Medrano, D., Thompson, R. C., Aldridge, D. C., 2015. Microplastics  
10 in freshwater systems: A review of the emerging threats, identification of  
11 knowledge gaps and prioritisation of research needs. *Water Research* 75,  
12 63–82.  
13  
14  
15 Fetter, C., 1994. *Applied hydrogeology*: Macmillan college publishing com-  
16 pany. New York New York.  
17  
18  
19 Fried, J. J., 1975. *Groundwater pollution*. Elsevier.  
20  
21 Galarneau, A., Guenneau, F., Gedeon, A., Mereib, D., Rodriguez, J., Fa-  
22 jula, F., Coasne, B., 2016. Probing interconnectivity in hierarchical mi-  
23 croporous/mesoporous materials using adsorption and nuclear magnetic  
24 resonance diffusion. *Journal of Physical Chemistry C* 120 (3), 1562–1569.  
25  
26  
27 Ginzburg, I., d’Humières, D., Kuzmin, A., 2010. Optimal stability of  
28 advection-diffusion lattice boltzmann models with two relaxation times  
29 for positive/negative equilibrium. *Journal of Statistical Physics* 139 (6),  
30 1090–1143.  
31  
32  
33 Gray, F., Boek, E., 2016. Enhancing computational precision for lattice boltz-  
34 mann schemes in porous media flows. *Computation* 4 (11).  
35  
36  
37 Gray, F., Cen, J., Boek, E., 2016. Simulation of dissolution in porous media  
38 in three dimensions with lattice boltzmann, finite-volume, and surface-  
39 rescaling methods. *Physical Review E* 94 (043320).  
40  
41  
42 Guo, L., Xiao, L., Shan, X., Zhang, X., 2016. Modeling adsorption with  
43 lattice boltzmann equation. *Scientific Reports* 6 (1), 1–9.  
44  
45  
46 Hlushkou, D., Gritti, F., Guiochon, G., Seidel-Morgenstern, A., Tallarek, U.,  
47 2014. Effect of adsorption on solute dispersion: A microscopic stochastic  
48 approach. *Analytical Chemistry* 86 (9), 4463–4470.  
49  
50  
51 Ichikawa, Y., Selvadurai, A., 2012. Transport phenomena in porous media,  
52 aspects of micro/macro behaviour. In: *Transport Phenomena in Porous  
53 Media, Aspects of Micro/Macro Behaviour*. Springer.  
54  
55  
56 Kahlen, M., Engel, A., Van den Broeck, C., 2017. Large deviations in taylor  
57 dispersion. *Physical Reviex E* 95 (012144).  
58  
59  
60  
61  
62  
63  
64  
65

- 1  
2  
3  
4  
5  
6  
7  
8  
9 Kwok, W., Hayes, R., Nasr-El-Din, H., 1995. Modelling dynamic adsorption  
10 of an anionic surfactant on berea sandstone with radial flow. *Chemical*  
11 *Engineering Science* 50 (5), 769–783.  
12  
13 Kwok, W., Nasr-El-Din, H., Hayes, R., Sethi, D., 1993. Static and dynamic  
14 adsorption of a non-ionic surfactant on berea sandstone. *Colloids and Sur-*  
15 *faces A: Physicochemical and Engineering Aspects* 78, 193–209.  
16  
17 Ladd, A., Verberg, R., 2001. Lattice-boltzmann simulations of particle-fluid  
18 suspensions. *Journal of Statistical Physics* 104 (516).  
19  
20 Levesque, M., Bénichou, O., Voituriez, R., Rotenberg, B., 2012. Taylor dis-  
21 persion with adsorption and desorption. *Physical Review E* 86 (3), 036316.  
22  
23 Levesque, M., Duvail, M., Pagonabarraga, I., Frenkel, D., Rotenberg, B.,  
24 2013. Accounting for adsorption and desorption in lattice boltzmann sim-  
25 ulations. *Physical Review E* 88 (1), 013308.  
26  
27 Manjhi, N., Verma, N., Salem, K., Mewes, D., 2006. Lattice boltzmann mod-  
28 elling of unsteady-state 2d concentration profiles in adsorption bed. *Chem-*  
29 *ical Engineering Science* 61 (8), 2510–2521.  
30  
31 Manoranjan, V. S., Stauffer, T. B., 1996. Exact solution for contaminant  
32 transport with kinetic langmuir sorption. *Water Resources Research* 32 (3),  
33 749–752.  
34  
35 Merks, R., Hoekstra, A., Sloot, P., 2002. The moment propagation method  
36 for advection-diffusion in the lattice boltzmann method: validation and  
37 pecllet number limits. *Journal of Computational Physics* 183 (563).  
38  
39 Ning, Y., Jiang, Y., Liu, H., Qin, G., 2015. Numerical modeling of slippage  
40 and adsorption effects on gas transport in shale formations using the lattice  
41 boltzmann method. *Journal of Natural Gas Science and Engineering* 26,  
42 345–355.  
43  
44 Payne, F. C., Quinnan, J. A., Potter, S. T., 2008. *Remediation hydraulics.*  
45 CRC Press.  
46  
47 Petersen, F., Hubbart, J. A., 2021. The occurrence and transport of mi-  
48 croplastics: The state of the science. *Science of the Total Environment*  
49 758 (143936).  
50  
51  
52  
53  
54  
55  
56  
57  
58  
59  
60  
61  
62  
63  
64  
65

- 1  
2  
3  
4  
5  
6  
7  
8  
9 Rolle, M., Le Borgne, T., 2019. Mixing and reactive fronts in the subsurface.  
10 Reviews in Mineralogy and Geochemistry 85 (1), 111–142.  
11  
12 Roque-Malherbe, R., 2018. Adsorption and diffusion in nanoporous materi-  
13 als. In: Adsorption and Diffusion in Nanoporous Materials. CRC Press.  
14  
15 Sahimi, M., 2012. Flow and transport in porous media and fractured rock.  
16 In: Flow and Transport in Porous Media and Fractured Rock. Wiley.  
17  
18 Sukop, M. C., Or, D., 2004. Lattice boltzmann method for modeling liquid-  
19 vapor interface configurations in porous media. Water Resources Research  
20 40 (1).  
21  
22 Talon, L., Bauer, D., Gland, N., Youssef, S., Auradou, H., Ginzburg, I.,  
23 2012. Assessment of the two relaxation time lattice-boltzmann scheme to  
24 simulate stokes flow in porous media. Water Resources Research 48 (4).  
25  
26 Vanson, J.-M., Boutin, A., Klotz, M., Coudert, F.-X., 2017a. Transport and  
27 adsorption under liquid flow: the role of pore geometry. Soft Matter 13 (4),  
28 875–885.  
29  
30 Vanson, J.-M., Coudert, F.-X., Klotz, M., Boutin, A., 2017b. Kinetic ac-  
31 cessibility of porous material adsorption sites studied through the lattice  
32 boltzmann method. Langmuir 33 (6), 1405–1411.  
33  
34 Vanson, J.-M., Coudert, F.-X., Rotenberg, B., Levesque, M., Tardivat, C.,  
35 Klotz, M., Boutin, A., 2015. Unexpected coupling between flow and ad-  
36 sorption in porous media. Soft Matter 11 (30), 6125–6133.  
37  
38 Wolanin, J., Barré, L., Dalmazzone, C., Bauer, D., 2021. A complete charac-  
39 terization of the structure of the vesicular phase in aot — brine system in  
40 the diluted region of the phase diagram. Colloids and Surfaces A: Physic-  
41 ochemical and Engineering Aspects 36 (8), 126098.  
42  
43 Wolanin, J., Barré, L., Dalmazzone, C., Frot, D., Jestin, J., Perrot, H., Bauer,  
44 D., 2020. Insight into kinetics and mechanisms of aot vesicle adsorption on  
45 silica in unfavorable conditions. Langmuir 36 (8), 1937–1949.  
46  
47 Wu, T., Zhang, D., 2016. Impact of adsorption on gas transport in nanopores.  
48 Scientific Reports 104, 23629.  
49  
50  
51  
52  
53  
54  
55  
56  
57  
58  
59  
60  
61  
62  
63  
64  
65

1  
2  
3  
4  
5  
6  
7  
8  
9  
10  
11  
12  
13  
14  
15  
16  
17  
18  
19  
20  
21  
22  
23  
24  
25  
26  
27  
28  
29  
30  
31  
32  
33  
34  
35  
36  
37  
38  
39  
40  
41  
42  
43  
44  
45  
46  
47  
48  
49  
50  
51  
52  
53  
54  
55  
56  
57  
58  
59  
60  
61  
62  
63  
64  
65

Xu, R., Prodanović, M., Landry, C. J., 2018. Simulation of gas adsorption and capillary condensation in shale nanopores using lattice boltzmann modeling. Unconventional Resources Technology Conference (URTEC).

Xu, R., Prodanović, M., Landry, C. J., 2019. Study of subcritical and supercritical gas adsorption behavior in different nanopore systems in shale using lattice boltzmann method. International Journal of Coal Geology 212, 103263.

Zaafouri, Z., Batôt, G., Nieto-Draghi, C., Rotenberg, B., Bauer, D., Coasne, B., 2021. Lattice boltzmann method for adsorption under stationary and transient conditions: Interplay between transport and adsorption kinetics in porous media. Physical Review E 104, 015314.

Zaafouri, Z., Bauer, D., Batôt, G., Nieto-Draghi, C., Coasne, B., 2020. Cooperative effects dominating the thermodynamics and kinetics of surfactant adsorption in porous media: From lateral interactions to surface aggregation. The Journal of Physical Chemistry B.

## Highlights

- The Lattice Boltzmann scheme is extended to complex adsorption behavior
- Micropollutants and surfactants follow complex aggregation effects on the surface
- Adsorption thermodynamics and kinetics strongly influence pollutant dispersion
- Different adsorption properties lead to specific transient régimes
- Langmuir adsorption leads to Taylor dispersion in the long-time range